Coexpression Networks Implicate Human Midfetal Deep Cortical Projection Neurons in the Pathogenesis of Autism

A. Jeremy Willsey,[1,2] Stephan J. Sanders,[1,2] Mingfeng Li,[3,4] Shan Dong,[1,5] Andrew T. Tebbenkamp,[3,4] Rebecca A. Muhle,[1,4,6] Steven K. Reilly,[1] Leon Lin,[7] Sofia Fertuzinhos,[3,4] Jeremy A. Miller,[8] Michael T. Murtha,[9] Candace Bichsel,[3,4] Wei Niu,[1,4,6] Justin Cotney,[1] A. Gulhan Ercan-Sencicek,[6,9] Jake Gockley,[1] Abha R. Gupta,[6,10] Wenqi Han,[3,4] Xin He,[11] Ellen J. Hoffman,[6,9] Lambertus Klei,[12] Jing Lei,[13] Wenzhong Liu,[1] Li Liu,[13] Cong Lu,[13] Xuming Xu,[3,4] Ying Zhu,[3,4] Shrikant M. Mane,[14] Ed S. Lein,[8] Liping Wei,[5,15] James P. Noonan,[1,4] Kathryn Roeder,[11,13] Bernie Devlin,[12,*] Nenad Sestan,[3,4,*] and Matthew W. State[1,2,6,9,16,*]

[1]Department of Genetics, Yale School of Medicine, New Haven, CT 06510, USA
[2]Department of Psychiatry, University of California, San Francisco, San Francisco, CA 94143, USA
[3]Department of Neurobiology, Yale School of Medicine, New Haven, CT 06510, USA
[4]Kavli Institute for Neuroscience, Yale School of Medicine, New Haven, CT 06510, USA
[5]Center for Bioinformatics, State Key Laboratory of Protein and Plant Gene Research, School of Life Sciences, Peking University, Beijing 100871, China
[6]Child Study Center, Yale School of Medicine, New Haven, CT 06510, USA
[7]Department of Computational Biology and Bioinformatics, Yale University, New Haven, CT 06511, USA
[8]Allen Institute for Brain Science, Seattle, WA 98103, USA
[9]Program on Neurogenetics, Yale School of Medicine, New Haven, CT 06510, USA
[10]Department of Pediatrics, Yale School of Medicine, New Haven, CT 06510, USA
[11]Ray and Stephanie Lane Center for Computational Biology, Carnegie Mellon University, Pittsburgh, PA 15213, USA
[12]Department of Psychiatry, University of Pittsburgh School of Medicine, Pittsburgh, PA 15213, USA
[13]Department of Statistics, Carnegie Mellon University, Pittsburgh, PA 15213, USA
[14]Yale Center for Genomic Analysis, Yale School of Medicine, New Haven, CT 06417, USA
[15]National Institute of Biological Sciences, Beijing 102206, China
[16]Department of Psychiatry, Yale School of Medicine, New Haven, CT 06510, USA
*Correspondence: devlinbj@upmc.edu (B.D.), nenad.sestan@yale.edu (N.S.), matthew.state@ucsf.edu (M.W.S.)
http://dx.doi.org/10.1016/j.cell.2013.10.020

SUMMARY

Autism spectrum disorder (ASD) is a complex developmental syndrome of unknown etiology. Recent studies employing exome- and genome-wide sequencing have identified nine high-confidence ASD (hcASD) genes. Working from the hypothesis that ASD-associated mutations in these biologically pleiotropic genes will disrupt intersecting developmental processes to contribute to a common phenotype, we have attempted to identify time periods, brain regions, and cell types in which these genes converge. We have constructed coexpression networks based on the hcASD "seed" genes, leveraging a rich expression data set encompassing multiple human brain regions across human development and into adulthood. By assessing enrichment of an independent set of probable ASD (pASD) genes, derived from the same sequencing studies, we demonstrate a key point of convergence in midfetal layer 5/6 cortical projection neurons. This approach informs when, where, and in what cell types mutations in these specific genes may be productively studied to clarify ASD pathophysiology.

INTRODUCTION

Autism spectrum disorders (ASDs) are defined by impairments in reciprocal social interaction, often accompanied by abnormalities in language development as well as repetitive behaviors and/or restricted interests. Considerable genetic and phenotypic heterogeneity has complicated efforts to establish the biological substrates of the syndrome. However, a sea change is currently underway in the genetics and genomics of ASD. Although genome-wide efforts to identify common genetic variation contributing to the syndrome have not yet led to reproducible results (State and Levitt, 2011), the identification of the important contribution of rare de novo mutations (Jamain et al., 2003; Sanders et al., 2011; Sebat et al., 2007) combined with high-throughput sequencing technology has recently led to the systematic discovery of de novo loss of function (LoF) mutations carrying comparatively large biological effects in ASD (Iossifov et al., 2012; Kong et al., 2012; Neale et al., 2012; O'Roak et al., 2011, 2012a, 2012b; Sanders et al., 2012). As a result, the set of associated genes has increased markedly

during the past 18 months, and this number will continue to grow steadily and predictably as additional cohorts of ASD families are sequenced (Buxbaum et al., 2012). Moreover, recent advances are further clarifying the genomic architecture of ASD. Although de novo point mutations have so far been estimated to play a contributory role in approximately 15% of affected individuals, estimates of locus heterogeneity imparted by these mutations alone already range from several hundred to more than 1,000 genes (He et al., 2013; Iossifov et al., 2012; Sanders et al., 2012).

The increasing number of genes carrying rare coding mutations with strong association to the human phenotype presents unprecedented opportunities for translational neuroscience. At the same time, the combination of extraordinary locus heterogeneity and biological pleiotropy poses considerable obstacles to the dissection of the pathophysiology of ASD, including the challenge of designing productive functional studies for a given gene in the absence of knowing when and where in the brain to investigate the identified risk mutations. This issue is particularly relevant given the fact that many of the genes discovered to date are involved in multiple biological processes at multiple points during development. Moreover, identical mutations in the same gene can lead to widely disparate psychiatric and neurological syndromes (Malhotra and Sebat, 2012). Consequently, a determination of spatiotemporal convergence among groups of disease-related mutations, all known to lead to ASD, may be particularly helpful as a first step toward identifying the functional perturbations specifically relevant for this phenotype.

With this in mind, we have set out to address the key question of if and when, in what brain regions, and in which cell types specific groups of ASD-related mutations converge during human brain development. To pursue this question, we have taken a "bottom-up" approach to gene coexpression network analysis, focusing initially on only nine "seed" genes carrying multiple de novo LoF mutations and thereby showing the strongest evidence for association with ASD. By focusing on these nine "high-confidence" ASD (hcASD) genes, we have sought to minimize the noise that can accompany network analyses based on inputs with widely varying evidence for association. Moreover, we have restricted input genes to those identified only via "hypothesis-naïve" exome- and genome-wide sequencing and have set a consistent statistical threshold for inclusion, minimizing the confounds that may accompany attempts to clarify mechanism using inputs that may have been identified, in part, based on their biological plausibility.

To evaluate these nine seed genes, we have used spatially and temporally rich mRNA expression data from developing human brain as the substrate for constructing networks. This choice is based on several key considerations: first, that an analysis of the expression trajectories of ASD-associated genes in typically developing human brain can provide insight into normal biological mechanisms that go awry in ASD (State and Sestan, 2012); second, that highly correlated gene expression is likely to reflect shared function and/or regulation; and third, and perhaps most importantly, that recent work in characterizing the human brain transcriptome underscores the spatial and temporal dynamism that occurs during development and provides the ability to exploit this dimensionality (Kang et al., 2011). These types of

data are not yet available for protein-protein interaction and gene-ontology databases.

To search for points of convergence among spatially and temporally defined coexpression networks, we relied on a second, nonoverlapping set of probable ASD (pASD) genes found to carry a single de novo LoF mutation and derived from the same studies as those yielding the hcASD seed genes. This inclusion criterion was likewise designed to minimize selection bias and batch effects and to provide relatively uniform independent evidence for association with ASD across this set of inputs.

Our analysis identifies robust, statistically significant evidence for convergence of the input set of hcASD and pASD risk genes in glutamatergic projection neurons in layers 5 and 6 of human midfetal prefrontal and primary motor-somatosensory cortex (PFC-MSC). Given the extensive genetic and phenotypic heterogeneity underlying ASD and the small fraction of risk genes that we have examined in this study, this likely represents only one of several such points of convergence. Nonetheless, the analytic approach presented here clarifies key variables relevant for productive functional studies of specific ASD genes carrying LoF mutations, providing an important step in moving from gene discovery to an actionable understanding of ASD biology.

RESULTS

Identification of hcASD Seed Genes

To identify input genes for this analysis, we have consolidated a cohort of 1,043 families (599 quartets, 444 trios) from a combination of published data (987 families; 543 quartets, 444 trios) (Iossifov et al., 2012; Kong et al., 2012; Neale et al., 2012; O'Roak et al., 2012b) and exome sequencing of an additional 56 quartets from the Simons Simplex Collection (SSC), a well-characterized ASD cohort consisting of families with one affected proband, two unaffected parents, and, in the majority of pedigrees, at least one unaffected sibling (Fischbach and Lord, 2010). Among the 1,043 probands, 144 de novo LoF mutations were identified (Table S1 available online), with LoF defined as a premature stop codon, canonical splice-site disruption, or frameshift insertion/deletion. Within the 599 quartets from the SSC (Iossifov et al., 2012; Sanders et al., 2012), we observed 75 de novo LoF mutations in 72 of the affected probands compared to 34 in 32 of the unaffected matched sibling controls (odds ratio [OR] 2.21 95% confidence interval [CI]: 1.45-3.36; $p = 5 \times 10^{-5}$, binomial exact test; Figure S1; Table S1).

Based on this data set, the observation of three de novo LoF mutations in the same gene in unrelated individuals identifies an ASD gene (false discovery rate [FDR] q = 0.0002; >99.9% chance of being a true ASD gene). Moreover, genes with two or more de novo LoF mutations are also very likely to be true ASD genes (q = 0.02; 97.8% chance of being a true ASD gene). Thus, we refer to genes with two or more de novo LoF mutations in unrelated individuals as hcASD genes. Finally, we find that genes carrying a single de novo LoF mutation are more likely than not to be true ASD genes (q = 0.45; 54.7% chance of being a true ASD gene). We subsequently refer to these as probable ASD (pASD) genes. Overall, our analysis of the 1,043 families identifies one previously unreported hcASD gene with two de novo LoF mutations: *Ankyrin 2, neuronal* (*ANK2*); confirms eight

other hcASD genes (Figure 1A); and identifies 122 pASD genes (Table S1).

Constructing Spatiotemporal Coexpression Networks

To interrogate coexpression dynamics of the nine hcASD genes in the context of human brain development, we utilized a previously published spatially and temporally rich transcriptome data set (Kang et al., 2011) generated as part of the BrainSpan project. These exon-level expression data originate from 16 regions of the human brain sampled in 57 clinically unremarkable postmortem brains of diverse ancestry (31 males, 26 females) that span 15 consecutive periods of neurodevelopment and adulthood from 5.7 postconceptual weeks (PCW) to 82 years (Figures 1B and 1C).

To identify specific time points and regions of brain development relevant to ASD, we partitioned the data into developmental periods and subsets of brain regions. Temporally, we used a sliding window of three consecutive time periods across the 15 total periods, producing 13 windows. Spatially, our preliminary analysis (Figure S2A) suggested that clustering the brain regions based on transcriptome data from fetal development (period 3–7) would optimize resolution. Therefore, brain regions with high transcriptional similarity were identified using hierarchical clustering of fetal transcriptome data. Four main clusters were observed (Figure 2A): (1) V1C, ITC, IPC, A1C, and STC (V1C-STC cluster); (2) M1C, S1C, VFC, MFC, DFC, and OFC (prefrontal and primary motor-somatosensory cortex or PFC-MSC cluster); (3) STR, HIP, and AMY; and (4) MD and CBC (MD-CBC cluster). In total, we generated 52 gene coexpression networks (13 time windows by four anatomical clusters), corresponding to 52 spatiotemporal windows (Figure 1D). These networks were created by calculating pairwise Pearson correlation coefficients between each of the nine hcASD genes and 16,947 genes from the exon array data set. To focus on the most relevant coexpression partners, we identified the 20 coexpressed genes best correlated to each hcASD gene (Figure 1E) and having a correlation coefficient $\geq$ 0.7.

pASD Gene Enrichment Is Localized to Specific Spatiotemporal Networks

We reasoned that if a particular coexpression network captures ASD-related biology, then we would expect to see additional ASD genes mapping within that network. Consequently, to determine whether any of the 52 spatiotemporal networks showed convergence of ASD gene expression, we first asked whether any showed a statistically significant enrichment of pASD genes (Figure 1F) based on a hypergeometric test.

We identified enrichment of pASD genes in just 4 of the 52 networks (Figure 2B), after Bonferroni correction for multiple testing: PFC-MSC in period 3–5 (10–19 PCW; $p = 9.9 \times 10^{-6}$); PFC-MSC in period 4–6 (13–24 PCW; $p = 1.2 \times 10^{-3}$); V1C-STC in period 7–9 (24 PCW to 12 months of age; $p = 0.02$); and MD-CBC in period 8–10 (birth to 6 years of age; $p = 3.5 \times 10^{-4}$).

Permutation Testing Highlights Networks Derived from Midfetal Prefrontal and Primary Motor-Somatosensory Cortex

Although the hypergeometric test is a computationally efficient approach to an initial evaluation of enrichment, it assumes that all genes have an equal chance of being found in the network; however, the rate of de novo LoF mutations varies with gene size and GC content, violating this assumption. Moreover, the correlation-based network construction could potentially lead to inflated p values. Thus, we conducted separate permutation tests with 100,000 iterations for each of the four putatively enriched networks (Figure 2C). In each iteration, we randomly selected nine hcASD seed genes, with the probability of seed gene selection based on gene size and GC content, and then constructed the corresponding coexpression network using the identical criteria noted above. We then quantified the presence of pASD genes within each network and assessed the significance of the observed enrichment, correcting for multiple comparisons. Using this more stringent permutation test (Figure 2C), pASD enrichment remained in the PFC-MSC networks at periods 3–5 (p = 0.003) and 4–6 (p = 0.05) and in the MD-CBC network at period 8–10 (p = 0.04). Enrichment was no longer observed in the fourth (period 7–9) network. Because the MD-CBC network had relatively few tissue samples available compared with the PFC-MSC networks at periods 3–5 and 4–6 (26, 107, and 140 samples, respectively; Figure S2F), we elected to focus our subsequent analyses on the two PFC-MSC networks, hereafter referred to as the "midfetal" networks. Additional permutation tests either varying the number of top coexpressed genes chosen or permuting the set of pASD genes instead of the hcASD genes, as well as a cross-validation experiment and a temporal analysis of individual periods, confirmed the robustness of our findings (Figures S2C–S2E; Table S2). The two midfetal networks are displayed in Figures 3A and 3B, the period 8–10 network is displayed in Figure S3, and network genes are summarized in Table S3.

The Midfetal Networks Capture Biologically Meaningful Data

Given the hypothesis that strongly correlated genes share regulation and/or function, we assessed whether the genes in the two midfetal networks had greater than expected similarity in their spatiotemporal expression patterns. As predicted, both the period 3–5 and 4–6 networks had particularly high correlation coefficients, reflecting networks more connected than expected by chance (p = 0.03 and p = 0.02, respectively; Figures 3A and 3B), suggesting that the genes within these networks are biologically related.

The most connected hcASD gene within the period showing the strongest evidence for convergence (period 3–5 network in PFC-MSC) was *T-box, brain, 1* (*TBR1*), a transcription factor known to be involved in forebrain development. Consequently, we assessed the relationship between *TBR1* and the other genes in this network. First, we investigated whether its perturbation altered expression of other network genes. Using whole mouse cortex isolated from *Tbr1*$^{-/-}$ and *Tbr1*$^{+/+}$ littermates at postnatal day 0 (P0, equivalent to human early midfetal development; Workman et al., 2013), we conducted RNA sequencing (RNA-seq) and identified differentially expressed (DEX) genes (Table S4). Four of these DEX genes were observed in the network; *NR4A2* and *SV2B* were both downregulated, whereas *FEZF2* and *NEFM* were both upregulated. Furthermore, all four DEX genes have previously been identified as TBR1 targets by
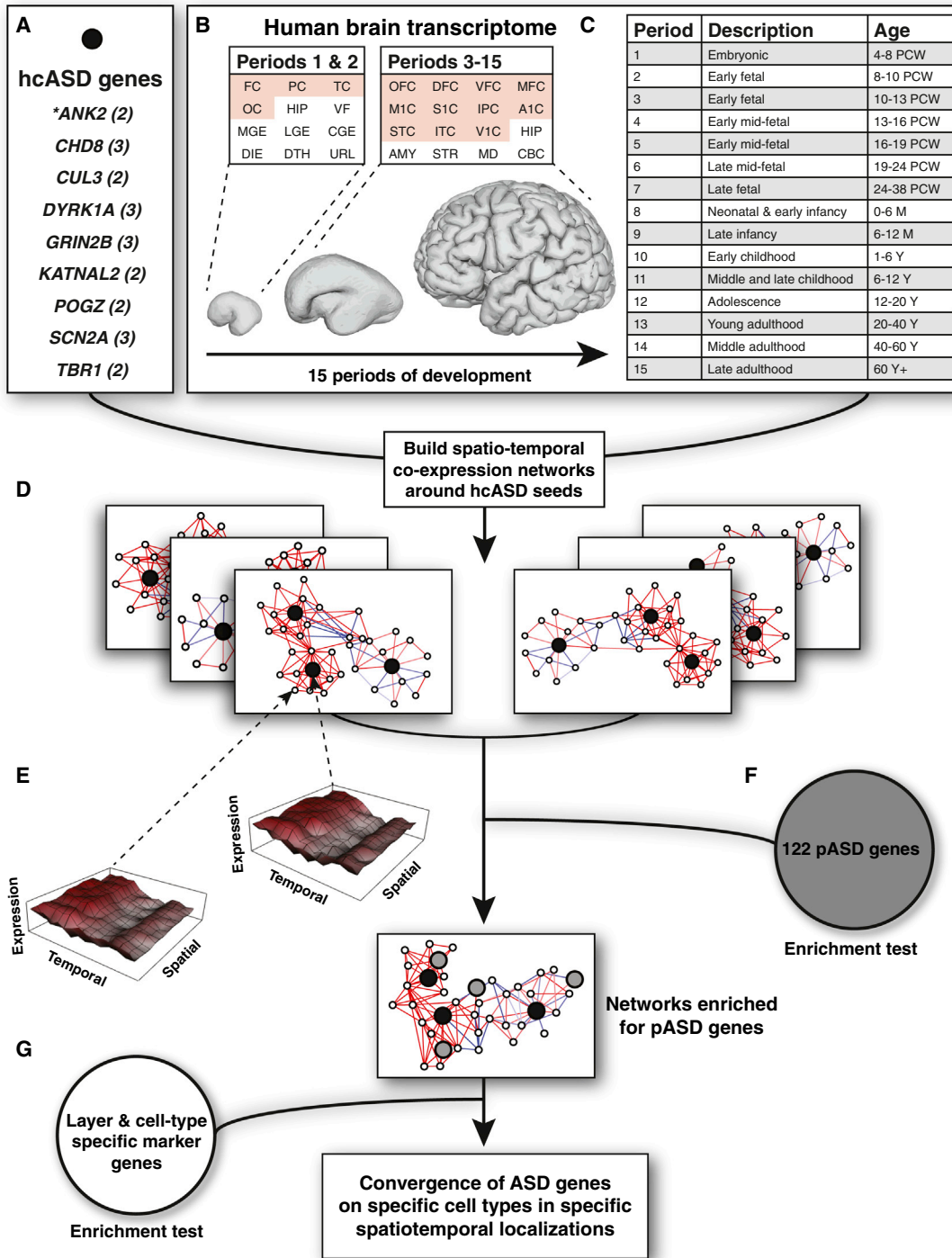
Figure 1. Overview of Coexpression Analysis Workflow and Associated Data Sets

(A) Nine hcASD genes derived from our data and additional published data sets. The number of independent de novo LoF mutations identified is indicated in parentheses. *ANK2* is a novel ASD-associated gene.

(B) A comprehensive data set of spatiotemporal gene expression spanning human brain development (Kang et al., 2011) was used to perform coexpression analysis. This data set spans 12 brain regions during periods 1 and 2 (embryonic and early fetal development) and 16 regions from period 3 to period 15 (early fetal to late adulthood). Neocortical regions are in red.

(C) Periods of human brain development as defined by Kang et al. (2011). PCW, postconceptual weeks; M, postnatal months; Y, postnatal years.

(D) The hcASD genes (black) are used as "seeds" to build coexpression networks along spatial and temporal dimensions.

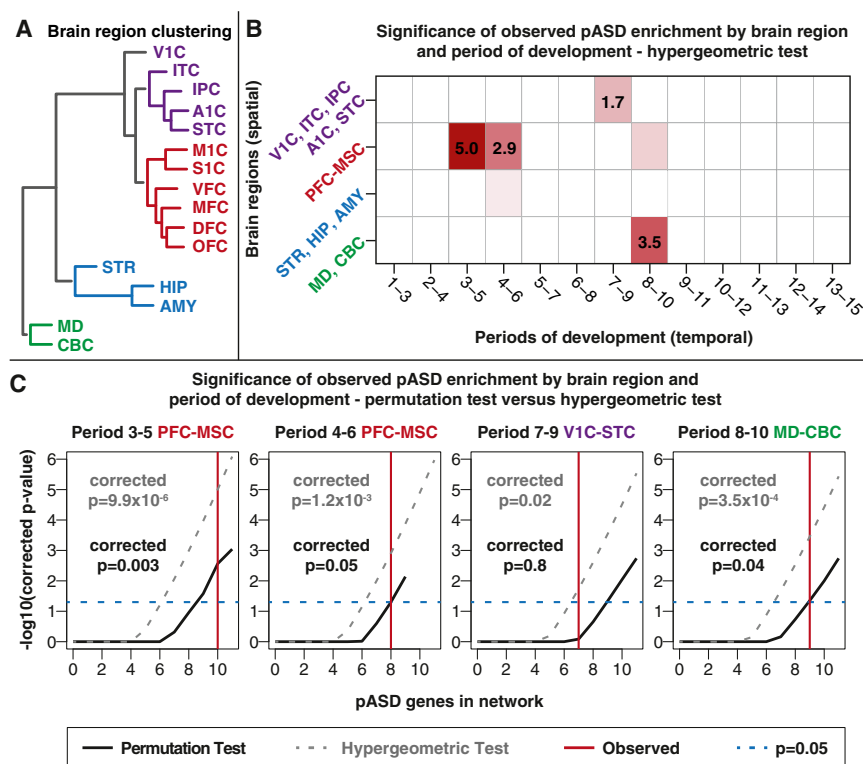*(legend continued on next page)*

Figure 2. Convergence in Prefrontal and Primary Motor-Somatosensory Cortex Regions during Midfetal Development

(A) Hierarchical clustering of brain regions based on transcriptional similarity during fetal development (periods 3–7) divides the brain regions into four groups, demarcated by color. These clusters also reflect actual topographical proximity and functional segregation.

(B) To achieve spatiotemporal resolution, coexpression networks were formed from 52 subsets of the expression data based on 13 developmental stages (in three period windows) and four sets of brain regions (clusters shown in A). Each of the networks was tested for enrichment of 122 pASD genes. This heatmap shows the negative $\log_{10}$(p value) (hypergeometric test) for enrichment in each network with developmental stages on the x axis and brain regions on the y axis. Networks that are not significant are in white; nominally significant networks are in light red; networks that are significant after correction for multiple comparisons are in red with the negative $\log_{10}$(p value) noted.

(C) pASD gene enrichment is statistically significant, after correction for multiple comparisons, by hypergeometric test (gray line) in the given regions and time points. Black lines show p values estimated from the permutation test based on the number of pASD genes within the networks (corrected for multiple comparisons); the vertical red line shows the number of pASD

genes observed for that specific network. pASD enrichment in period 3–5 (p = 0.003), 4–6 (p = 0.05), and 8–10 (p = 0.04) networks remains significant, whereas the period 7–9 network (p = 0.8) does not.

PFC-MSC, prefrontal cortex and primary motor-somatosensory cortex; V1C-STC, V1C, ITC, IPC, A1C, STC. See also Figure S2 and Table S2.

chromatin immunoprecipitation sequencing (ChIP-seq) analysis in N2A cells (Han et al., 2011). Given the regulatory function of TBR1 and its prominence in the midfetal networks, we evaluated if our results were primarily a result of inclusion of this gene. We found that this was not the case: removal of *TBR1* from the coexpression analysis did not alter any of our findings regarding spatiotemporal convergence (Figure S2B).

pASD Genes within Midfetal Networks Are More Likely to Be Associated with ASD

As noted, we estimate that over half of the 122 pASD genes represent true ASD risk genes. We consequently hypothesized that if the midfetal networks effectively capture ASD biology, then the pASD genes within these networks would show greater evidence of association with ASD compared to those

present in the 100,000 permuted networks. To test this, we turned to TADA, a newly developed statistical approach that integrates de novo and inherited variant data with estimates of gene mutability to yield gene-specific p values (He et al., 2013). TADA p values for each gene were calculated based on the whole-exome data in our study as well as case-control data (935 cases and 870 controls) from the ARRA Autism Sequencing Consortium study (Liu et al., 2013). Because all the pASD genes were defined by the presence of a single de novo LoF mutation, any variability in gene-specific p values derived from the TADA analysis represents independent evidence for association. Based on 100,000 permutations, we observed that the TADA p values for pASD genes within both midfetal networks were significantly lower than expected (Figures 3C and 3D).

(E) Mean expression levels for two genes are plotted as a function of period of development (temporal axis) and region of the brain (spatial axis). The images illustrate that highly correlated genes have similar expression profiles across these dimensions. The Pearson's correlation value quantifies the similarity between these profiles.

(F) Networks are interrogated for enrichment of an independent set of 122 probable ASD (pASD) genes (gray).

(G) Networks are tested for enrichment of layer- and cell-type-specific genes.

FC, frontal cerebral wall; PC, parietal cerebral wall; TC, temporal cerebral wall; OC, occipital cerebral wall; HIP, hippocampal anlage (periods 1–2), hippocampus (periods 3–15); VF, ventral forebrain; MGE, medial ganglionic eminence; LGE, lateral ganglionic eminence; CGE, caudal ganglionic eminence; DIE, diencephalon; DTH, dorsal thalamus; URL, upper (rostral) rhombic lip; OFC, orbital prefrontal cortex; DFC, dorsal prefrontal cortex; VFC, ventral prefrontal cortex; MFC, medial prefrontal cortex; M1C, primary motor cortex; S1C, primary somatosensory cortex; IPC, posterior inferior parietal cortex; A1C, primary auditory cortex; STC, superior temporal cortex; ITC, inferior temporal cortex; V1C, primary visual cortex; AMY, amygdala; STR, striatum; MD, mediodorsal nucleus of the thalamus; CBC, cerebellar cortex. See also Figure S1 and Table S1.

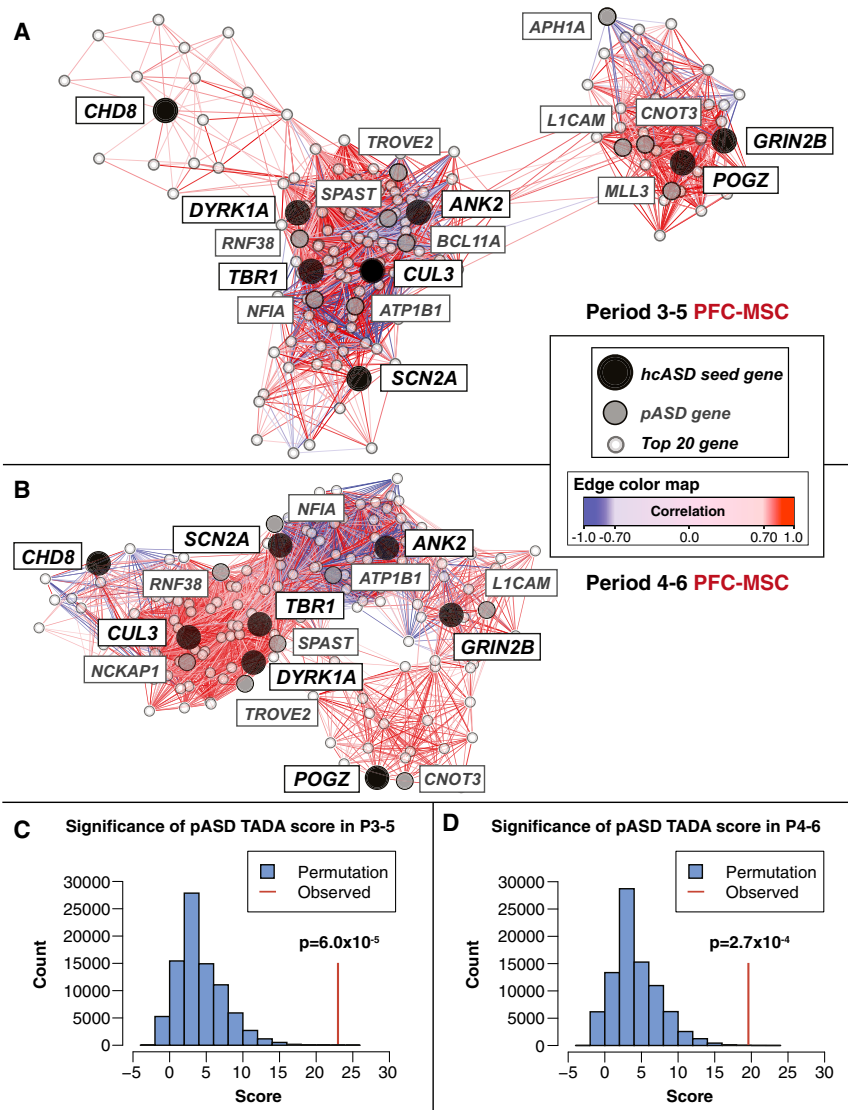(A and B) The period 3–5 (A) and period 4–6 (B) coexpression networks are displayed with the force-directed layout function of Cytoscape using correlation as the edge weight (Cline et al., 2007). Gene coexpression analysis included the 20 genes best correlated with each hcASD gene. The hcASD seed genes are in black; pASD genes identified within the network are in gray; and the top 20 coexpressed genes that are not pASD genes are in white. The lines (edges) reflect coexpression correlations ≥ 0.7, and the shade represents the strength of the correlation; positive correlations are in in red; negative correlations are in blue.

(C and D) The pASD genes enriched within the networks in (A) and (B) represent those with the highest probability of being true ASD genes. The TADA score combines de novo mutation data with inherited variant data from trios, rare variant case-control data, and estimates of mutation rate in order to estimate the probability of ASD association for each gene (He et al., 2013). The histograms show the results of permutation tests (100,000 iterations each) assessing the combined TADA score in the period 3–5 (C) and period 4–6 (D) networks; the observed scores, shown by the vertical red lines, are highly significant (p = 6.0 × 10^{-5} and p = 2.7 × 10^{-4}, respectively). See also Figure S3 and Tables S3 and S4.

Human Midfetal Laminar-Specific Expression Data Implicate Inner Cortical Plate in ASD
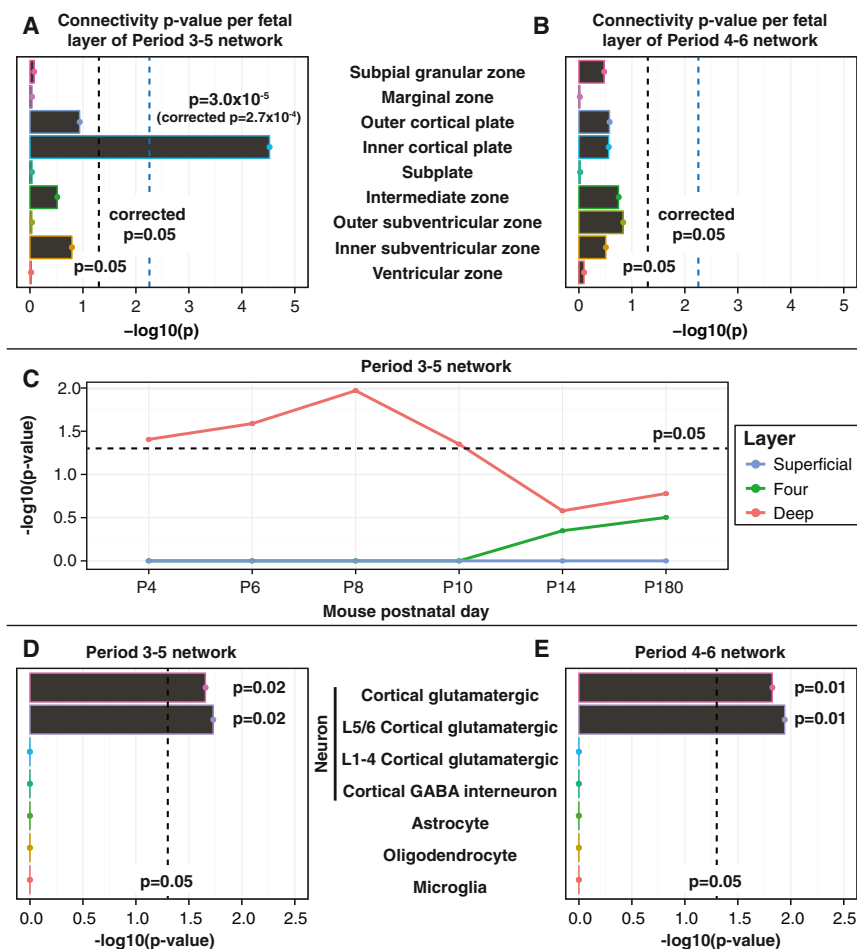
Given the well-established variability in gene expression by cortical layer, we reasoned that spatiotemporal networks identified in the PFC-MSC would reflect a heterogeneous signal from multiple layers within each dissection. Consequently, to increase the resolution of our analysis, we investigated whether the set of genes present in each midfetal network were more highly correlated within a particular cortical layer than expected by chance. Therefore, we utilized layer-specific microarray data that were obtained from laser microdissected (LMD) prenatal human brain by the BrainSpan Consortium (http://www.brainspan.org). Samples were derived from frontal neocortex of four brains, corresponding to periods 4, 5, or 6, and each region was dissected into nine layers, spanning from cortical surface to ventricular surface and including the outer (CPo) and inner (CPi) cortical plate.

To evaluate for layer specificity, we recreated both the midfetal periods 3–5 and 4–6 coexpression networks within each layer and assessed each layer-specific network for increased connectivity. This approach preserves the overall structure of the hcASD seed gene networks, including their temporal properties. Because many of the hcASD and pASD genes show expression throughout developing brain, we hypothesized that the expression dynamics of the ASD-related networks would be more informative than, for example, evaluating differential expression of individual genes. In practice, for each LMD layer, we calculated the Pearson's correlation coefficients for all gene pairs that were found to be present within the midfetal networks and then summed the coefficients within the layer to quantify network connectivity. The observed value was assessed using a permutation test and 100,000 iterations. We identified increased connectivity in a single layer, CPi, for the period 3–5 midfetal network (corrected p = 2.7 × 10^{-4}; Figures 4A and 4B; Figure S4).

Mouse Laminar-Specific Expression Data Implicate Deep Cortical Layers in ASD

Given the role of neuronal migration in early brain development, we considered whether the observed localization to CPi for the period 3–5 PFC-MSC network might change over time. Because the human LMD data were limited to a narrow developmental interval, we turned to a time series of neocortical layer-derived RNA-seq data for mouse brain development.

Figure 4. The PFC-MSC Networks Show Enrichment for Markers of Deep Layer Projection Neurons

(A and B) To improve the spatial resolution of the coexpression analysis, the midfetal networks were assessed in an independent prenatal transcriptome (http://www.brainspan.org) data set composed of microarray-based gene expression profiles of laser microdissected (LMD) human midfetal (period 4–6) brains. Each hcASD seed gene network was recreated within each layer from this LCM data and the significance of the observed connectivity (sum of correlations along network connections) for each layer was assessed by permutation test. The period 3–5 network (A) shows significant connectivity in the CPi region (inner cortical plate) corresponding to neocortical layers 5–6 (corrected $p = 2.7 \times 10^{-4}$), whereas the period 4–6 network (B) is not significantly connected in any layer.

(C) The period 3–5 PFC-MSC network is enriched for markers of deep layer cells in mouse cortex. At each postnatal day (P) indicated, differential gene expression analysis of RNA-seq data was performed on three cortical layers of two mouse cortices (one male, one female) to identify genes exclusively differentially expressed in a particular layer (markers). The "superficial" layer corresponds to the human marginal zone and CPo (human layer 2 [L2] and L3), layer "four" corresponds to human CPo (human L4), and the "deep" layer corresponds to human CPi and subplate (human L5/L6 and subplate). From P4 to P10 (mid- to late fetal development), human orthologs of murine deep layer marker genes are significantly enriched in the period 3–5 network (hypergeometric test). From P14 to P180 (adulthood), there is insufficient resolution to differentiate layers and none are significantly enriched.

(D and E) Enrichment of a set of previously published cell-type specific marker genes (Kang et al., 2011) is specific to cortical glutamatergic projection neurons (CPNs) in both midfetal networks (p = 0.02 for period 3–5; p = 0.01 for period 4–6). Markers of deep layer CPNs (L5/L6) are significantly enriched in both networks (p = 0.02 for period 3–5; p = 0.01 for period 4–6), whereas markers of superficial layer CPNs (L1 to L4) are not. All p values were assessed by permutation test with 100,000 iterations unless otherwise noted.
See also Figure S4 and Tables S5 and S6.

These data were composed of two mouse brains, one male and one female, for each of six time points from P4 to P180 (corresponding in humans to late midfetal development to adulthood; Workman et al., 2013). At each time point, we sampled three cortical zones: superficial layers (SL; L1 to L3), layer 4 (L4), and deep layers (DL; L5/L6) and identified genes that were upregulated in only one of these three zones (Table S5). We then assessed whether a greater than expected enrichment of these zone-specific genes was observed in the period 3–5 PFC-MSC network. Consistent with our findings in human fetal cortex, only deep-layer (L5/L6) markers showed enrichment (p < 0.04, hypergeometric test) and this enrichment was constrained to the earlier developmental time points P4 to P10 (equivalent to human late midfetal to late fetal; Figure 4C). This suggests that our finding of localization to CPi in human fetal brain for this hcASD-derived network was not a consequence of neurons that ultimately migrate to superficial cortical layers.

Gene-Marker-Based Analysis Implicates Layer 5/6 Glutamatergic Projection Neurons in ASD

Both the human fetal and mouse data localize the period 3–5 midfetal network to the deep layers of developing cortex. We next considered layer- and cell-specific gene markers to add a third, independent verification of this result and to increase our resolution to a specific cell type within the cortex. We utilized a previously published set of 40 marker genes representing five cell types and superficial and deep cortical layers in the developing human brain (Kang et al., 2011; Table S6). We assessed enrichment for these markers in the midfetal networks using permutation testing with 100,000 iterations. Significant enrichment was observed for cortical glutamatergic projection neurons (CPNs) in the period 3–5 and 4–6 networks (3 out of 17 markers in both; p = 0.02 and p = 0.01 for 3–5 and 4–6, respectively). Further inspection revealed that these three markers are specific for deep cortical layer (L5/L6) CPNs (3 out of 11 in both; p = 0.02 and p = 0.01 for 3–5 and 4–6, respectively; Figures 4D and 4E).
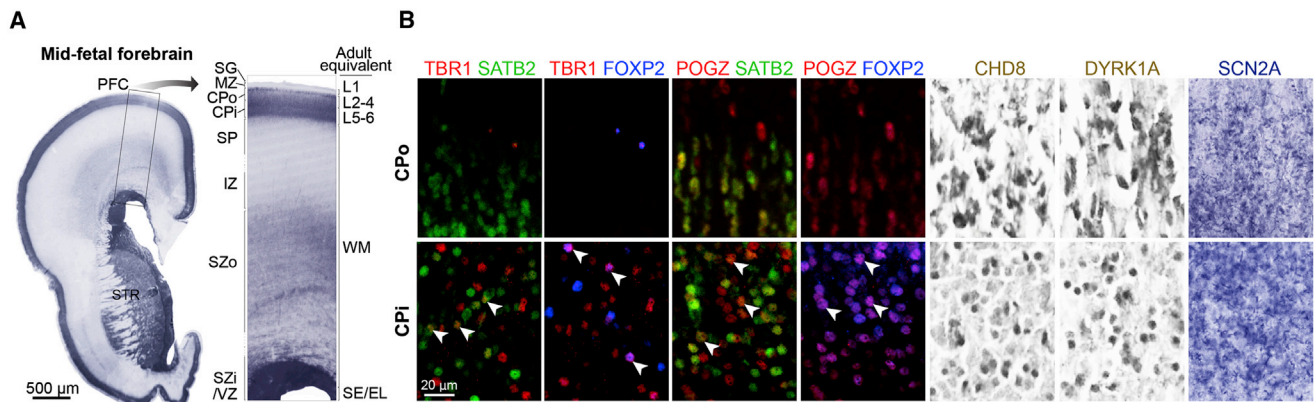
Figure 5. hcASD Genes Are Expressed in Midfetal Deep Layer Projection Neurons

(A) A coronal tissue section through the prefrontal cortex (PFC) and striatum (STR) of a midfetal forebrain was Nissl stained to visualize cells in distinct developmental zones. The darkest labeled zones are denser with cells, namely the VZ (ventricular zone) and SZi (inner subventricular zone), CPi (inner cortical plate), and CPo (outer cortical plate). The corresponding adult zones are labeled on the right of the higher magnified boxed area.

(B) Tissue sections of PFC areas at approximately equivalent ages (18–21 PCW) were stained with either antibodies (as labeled on top of the first six columns; fluorescence in red, green, or blue; DAB in brown) or in situ hybridization probes (last column, *SCN2A*). Images in the top row were taken at the boundary between CPo and MZ (marginal zone), and images in the bottom row at the boundary between CPi and SP (subplate). Arrows indicate cells colabeled for an hcASD gene and a marker gene (SATB2 or FOXP2).

SG, subpial granular zone; IZ, intermediate zone; SZo, outer subventricular zone; L, layer; WM, white matter; SE/EL, subependymal/ependymal layer.

Expression Profiling Confirms the Expression of hcASD Genes in Midfetal Cortical Projection Neurons

Our analysis of the ASD-associated midfetal networks predicts that the majority of the genes within the networks should be expressed in the CPi in midfetal prefrontal cortex. We tested this prediction by conducting immunostaining or in situ hybridization in period 5–6 coronal sections from human frontal cortex for five representative hcASD genes: *TBR1*, *POGZ*, *CHD8*, and *DYRK1A* (immunostaining) and *SCN2A* (in situ hybridization). As predicted, all five genes show robust expression in CPi projection neurons of this tissue (Figure 5). CHD8, DYRK1A, and *SCN2A* were observed in the majority of cortical plate neurons, including projection neurons in CPi and CPo. Consistent with our findings, *TBR1*, the most connected gene in our period 3–5 network, is exclusively expressed in CPi projection neurons in these developmental periods (Kwan et al., 2012). However, we note the expression of most other genes in the networks is not expected to be restricted to the CPi, as the association with this layer was observed at the network level.

To determine localization in different types of CPNs, we performed double immunofluorescent labeling using antibodies against the proteins encoded by the hcASD genes *TBR1* and *POGZ*, along with two well-known markers for subtypes of CPNs, FOXP2 and SATB2 (Kwan et al., 2012). Both TBR1 and POGZ colocalized with FOXP2, a marker of deep-layer subcortical projection neurons that is exclusively present in the CPi. In addition, in some CPi neurons, we observed TBR1 and POGZ colocalizing with SATB2, a marker of intracortical (corticocortical) projection neurons, indicating that both subgroups of CPi projection neurons express *TBR1* and *POGZ*.

DISCUSSION

The complexity of the genetic contribution to common neuropsychiatric conditions, including ASD, poses ample challenges for translational neuroscience. We sought to address some of these challenges by focusing on key questions that other analytical approaches have been hard pressed to tackle: specifically, when, where, and in what cell type should a specific ASD-related mutation or group of mutations be studied to begin to identify relevant pathophysiological mechanisms?

Given recent studies suggesting that as many as 1,000 genes or more could contribute to ASD (He et al., 2013; Iossifov et al., 2012; Sanders et al., 2012), our analysis has uncovered a surprising degree of developmental convergence. Despite starting with only nine hcASD seed genes, we have identified highly significant and robust evidence for the contribution of coexpression networks relevant to L5 and L6 CPNs in two overlapping periods of midfetal human development (3–5 and 4–6) corresponding to 10–24 PCW. These results strongly support the hypothesis that the marked locus heterogeneity underlying ASD will point to a much smaller set of underlying pathophysiological mechanisms.

Although there is clear evidence for the role of synaptic proteins in the pathogenesis of ASD, these findings point to the contribution of mechanisms extending beyond the synapse (State and Sestan, 2012). The identification of a functionally diverse set of risk genes within ASD networks, encoding proteins that are found in distinct cell compartments, is consistent with the hypothesis that alterations in multiple distinct pathways or processes may lead to the ASD phenotype by virtue of their spatial and temporal properties. For example, the CPi projection neurons of the midfetal PFC-MSC are among the first cortical neurons to form synaptic connections, and these early neural circuits may be particularly vulnerable to a variety of genetic perturbations and related functional disturbances that may all ultimately increase the risk for ASD.

To maximize the accuracy of our analysis, we focused considerable attention on the selection of input data. As noted, we

restricted seed genes to those carrying multiple de novo LoF mutations and pASD genes to those carrying a single de novo LoF mutation, all derived from the same set of sequencing studies. Although this excluded several previously identified and well-established ASD genes, it established statistically based and consistent inclusion criteria, provided input data with relatively uniform evidence for involvement in ASD, and removed any bias introduced by the selection of genes that may have been originally identified, in part, by mechanistic hypotheses.

Similarly, although the evidence for vulnerability in some aspect of development of midfetal CPNs in ASD is quite robust, there is also support for the notion that additional points of convergent biology will ultimately be found in ASD. For example, in addition to midfetal cortical development, we have identified preliminary evidence for pASD enrichment in thalamus and cerebellum during postnatal development. Notably, two previously well-established ASD genes, *NRXN1* and *NLGN4X*, also are found within this coexpression network (Figure S3). In a similar vein, we note that none of the well-established syndromic ASD genes, such as *FMR1*, *TSC1*, *TSC2*, or *PTEN*, are found in the networks highlighted by our analyses. Taken together, these findings suggest that additional time points and brain regions are likely to be identified as both the number of bona fide risk genes grows and the depth of data on the molecular landscape of human brain development increases.

In this regard, we note the overall similarities between our findings and those reported in the accompanying study by Parikshak et al. (2013) in this issue of *Cell*, which uses an alternative approach to identify spatial and temporal convergence in genes involved in neurodevelopmental disorders. They also identify a potential role of CPNs in ASD, including in midfetal development and in L5/L6, yet their results also implicate L2/L3 in ASD. This difference is unsurprising, given differences in the input genes selected, in their approach to network/module construction and in their selection of expression data sets. By using a select small set of hcASD genes, our approach prioritized specificity over sensitivity, and we fully anticipated there would be undetected points of temporal and spatial convergence in ASD risk.

Nonetheless, the findings presented here immediately constrain important variables in the study of specific ASD-related mutations and provide the basis to pursue well-informed hypotheses regarding which mutations in which genes would be most likely to show overlapping molecular, cellular, or circuit-level phenotypes. Given the increasing pool of ASD genes and mutations and the wide range of biological processes the encoded proteins perform, this ability to focus future in vitro and in vivo studies on subsets of genes based on their spatial and temporal properties and network relationships promises to have considerable value in the pursuit of a deeper understanding of pathophysiological mechanisms as well as in the identification of treatment targets.

EXPERIMENTAL PROCEDURES

For more details on any of these sections, please see the Extended Experimental Procedures. All experiments involving animals were performed in accordance with a protocol approved by Yale University's Committee on Animal Research.

Exome Data and Mutations

Whole-blood-derived DNA for 56 families chosen at random from the Simons Simplex Collection was subjected to exon capture using the Nimblegen EZ Exome V2.0 array and sequenced with 74 bp paired-end reads on the Illumina HiSeq 2000. Sequence reads were aligned to hg19 using BWA (Li and Durbin, 2009). Single-nucleotide variants were predicted using SAMtools (Li et al., 2009), whereas insertion-deletions were predicted using local realignment with Dindel (Albers et al., 2011). All de novo variants were confirmed using PCR and Sanger sequencing. Additional mutation data were obtained from the supplemental material from published papers (Iossifov et al., 2012; Kong et al., 2012; Neale et al., 2012; O'Roak et al., 2012a, 2012b; Sanders et al., 2012).

Construction of Spatiotemporal Coexpression Networks

Gene-level expression data (Platform GPL5175; Affymetrix GeneChip Human Exon 1.0 ST Array) were downloaded from the National Center for Biotechnology Information (NCBI) Gene Expression Omnibus (GEO accession number GSE25219) (Kang et al., 2011). Expression data from the core probe set were used in coexpression analysis (exceptions: for hcASD gene *CHD8* and the pASD genes *FLG*, *FREM3*, *FRG2C*, *LMTK3*, *THSD7A*, *UBN2*, and *ZNF594*, data from the extended probe set were utilized). Within each postmortem brain, gene expression values were determined per region, resulting in a vector of expression values (expression profile) for each gene by brain region and brain sample. Within each spatiotemporal window, the expression profile was trimmed to relevant regions and brain samples only, and the Pearson correlation coefficient for the trimmed expression profile was calculated for each pairwise combination of genes. For each seed gene, the top 20 best-correlated genes with an absolute correlation coefficient with the seed gene of ≥ 0.7 were selected; each network is composed of the hcASD genes and their top correlated genes. Edges are then formed between any network genes with absolute correlation coefficient ≥ 0.7. Any hcASD genes without edges were removed.

Temporal windows were determined solely by creating overlapping sets of three consecutive periods of development, starting with periods 1–3 and ending at periods 13–15. To determine spatial windows, brain regions were grouped according to transcriptional similarity during fetal development (periods 3–7): based on pairwise Spearman correlations, brain regions were hierarchically clustered in R using the "hclust" function ($1 - \text{corr}^2$ as the distance, clustering using Ward's method).

Permutation Tests

The permutation tests used throughout are based on selecting nine pseudo-hcASD seed genes weighted on the likelihood of observing multiple de novo LoF mutations by chance. A total of 100,000 sets of nine pseudo-hcASD genes were identified and separate coexpression networks were built for each of the four networks assessed. These 100,000 networks were used as the basis for the following permutation tests: pASD gene enrichment, connectivity, TADA p values, layer-specific marker genes, and cell-type-specific marker genes.

TBR1 KO mRNA-Seq and Data Analysis

Total RNA was isolated from freshly dissected P0 neocortices of a single set of $Tbr1^{-/-}$ and $Tbr1^{+/+}$ littermates using a QIAGEN RNeasy Mini Kit. Libraries were prepared using an Illumina mRNA-Seq Sample Prep Kit. Amplified cDNA was size-selected at 250 bp and validated using the Agilent Bioanalyzer DNA 1000 system. The final product was subjected to cluster generation using an Illumina Standard Cluster Generation Kit v4. Libraries were sequenced to generate 74 bp single-end reads using the Illumina Genome Analyzer pipeline. Differentially expressed genes were identified based on a |log2(fold change)| ≥ 0.5 and adjusted p ≤ 0.05 based on Fisher's exact test.

Network Analysis with Human Laminar-Specific Expression Data

Region- and layer-specific gene expression data were obtained from the BrainSpan Prenatal LMD Microarray project. This data set profiles gene expression in four brains spanning period 4–6 of development (15–21 PCW; see technical white paper at http://www.brainspan.org). To assess the

relevance of the two networks to each of the nine fetal layers or compartments, we determined normed Pearson's correlation coefficients between network genes connected in the original midfetal networks, using expression data from each layer separately. By summing these correlations, we were able to estimate the overall connectivity of the networks layer-by-layer and then to assess the significance of this connectedness using a permutation test with 100,000 iterations.

Enrichment Analysis in Mouse Neocortical Layers across Development

Different layers of the mouse cerebral neocortex were microdissected from live tissue sections of the *Dcdc2a-Gfp* transgenic reporter mouse (obtained from the GENSAT project; Schmidt et al., 2013), which expresses GFP selectively in L4 pyramidal and stellate glutamatergic excitatory neurons. Tissue samples were collected from the primary somatosensory area (equivalent to human S1C) of mouse brains at P4, P6, P8, P10, P14, and P180. Three laminar zones were isolated at each time point: superficial layers (SL; L2/L3 including marginal zone or L1, and pia), L4, and deep layers (DL; L5/L6 including transient subplate zone or adult white matter). At each time point, genes exclusively upregulated in only one laminar zone (marker genes) were identified.

Immunostaining and In Situ Hybridization

Coronal sections from 17–20 PCW human frontal cortex were used to validate the cellular resolution of ASD gene expression. For immunohistochemistry, sections were pretreated with 0.3% H_2O_2 followed by incubation in blocking buffer at room temperature and then incubation for 24–48 hr at 4°C in primary antibodies. Tissue was then incubated with biotin-labeled secondary antibodies, conjugated with avidin-biotin-peroxidase complex (Vector Laboratories), and visualized with DAB (Vector Laboratories). Images were taken using a digital scanner (Aperio ScanScope).

Immunofluorescent staining was performed similarly as aforementioned, without peroxide pretreatment, and with longer incubations in blocking buffer, primary and secondary antibodies, and intermittent washes. DAPI was included during incubation with secondary antibodies to counterstain nuclei.

For in situ hybridization, brain sections were first mounted on charged slides, followed by postfixation in 4% paraformaldehyde-PBS and then a 0.1 M triethanolamine with 0.25% acetic anhydride pretreatment. Sections were then incubated overnight at 65°C with 500 ng/ml of digoxigenin (DIG)-labeled cRNA probes corresponding to human *SCN2A* nucleotides 1,817–2,954 (NM_001040143). Sections were washed and incubated overnight at 4°C with alkaline phosphatase-conjugated anti-DIG antibodies, followed by signal detection using NBT/BCIP chromogen (Roche) diluted in a polyvinyl alcohol (PVA) buffer.

ACCESSION NUMBERS

The whole-exome sequence data from the additional 56 quartets reported in this paper are available from the Sequence Read Archive (SRA) of the NCBI under BioProject PRJNA224099. The *Tbr1*$^{-/-}$ *and Tbr1*$^{+/+}$ RNA-seq data reported in this paper are available from the SRA under BioProject PRJNA224108. The longitudinal neocortical layer-derived RNA-seq data for mouse brain development reported in this paper are available from the SRA under BioProject PRJNA224095.

SUPPLEMENTAL INFORMATION

Supplemental Information includes Extended Experimental Procedures, four figures, and six tables and can be found with this article online at http://dx.doi.org/10.1016/j.cell.2013.10.020.

ACKNOWLEDGMENTS

REFERENCES

Albers, C.A., Lunter, G., MacArthur, D.G., McVean, G., Ouwehand, W.H., and Durbin, R. (2011). Dindel: accurate indel calls from short-read data. Genome Res. *21*, 961–973.

Buxbaum, J.D., Daly, M.J., Devlin, B., Lehner, T., Roeder, K., State, M.W., and Consortium, T.A.S.; Autism Sequencing Consortium. (2012). The autism sequencing consortium: large-scale, high-throughput sequencing in autism spectrum disorders. Neuron *76*, 1052–1056.

Cline, M.S., Smoot, M., Cerami, E., Kuchinsky, A., Landys, N., Workman, C., Christmas, R., Avila-Campilo, I., Creech, M., Gross, B., et al. (2007). Integration of biological networks and gene expression data using Cytoscape. Nat. Protoc. *2*, 2366–2382.

Fischbach, G.D., and Lord, C. (2010). The Simons Simplex Collection: a resource for identification of autism genetic risk factors. Neuron *68*, 192–195.

Han, W., Kwan, K.Y., Shim, S., Lam, M.M., Shin, Y., Xu, X., Zhu, Y., Li, M., and Sestan, N. (2011). TBR1 directly represses Fezf2 to control the laminar origin and development of the corticospinal tract. Proc. Natl. Acad. Sci. USA *108*, 3041–3046.

He, X., Sanders, S.J., Liu, L., De Rubeis, S., Lim, E.T., Sutcliffe, J.S., Schellenberg, G.D., Gibbs, R.A., Daly, M.J., Buxbaum, J.D., et al. (2013). Integrated model of de novo and inherited genetic variants yields greater power to identify risk genes. PLoS Genet. *9*, e1003671.

Iossifov, I., Ronemus, M., Levy, D., Wang, Z., Hakker, I., Rosenbaum, J., Yamrom, B., Lee, Y.H., Narzisi, G., Leotta, A., et al. (2012). De novo gene disruptions in children on the autistic spectrum. Neuron *74*, 285–299.

Jamain, S., Quach, H., Betancur, C., Råstam, M., Colineaux, C., Gillberg, I.C., Soderstrom, H., Giros, B., Leboyer, M., Gillberg, C., and Bourgeron, T.; Paris Autism Research International Sibpair Study. (2003). Mutations of the X-linked genes encoding neuroligins NLGN3 and NLGN4 are associated with autism. Nat. Genet. *34*, 27–29.

Kang, H.J., Kawasawa, Y.I., Cheng, F., Zhu, Y., Xu, X., Li, M., Sousa, A.M.M., Pletikos, M., Meyer, K.A., Sedmak, G., et al. (2011). Spatio-temporal transcriptome of the human brain. Nature *478*, 483–489.

Kong, A., Frigge, M.L., Masson, G., Besenbacher, S., Sulem, P., Magnusson, G., Gudjonsson, S.A., Sigurdsson, A., Jonasdottir, A., Jonasdottir, A., et al. (2012). Rate of de novo mutations and the importance of father's age to disease risk. Nature *488*, 471–475.

Kwan, K.Y., Sestan, N., and Anton, E.S. (2012). Transcriptional co-regulation of neuronal migration and laminar identity in the neocortex. Development *139*, 1535–1546.

Li, H., and Durbin, R. (2009). Fast and accurate short read alignment with Burrows-Wheeler transform. Bioinformatics *25*, 1754–1760.

Li, H., Handsaker, B., Wysoker, A., Fennell, T., Ruan, J., Homer, N., Marth, G., Abecasis, G., Durbin, R., and Subgroup, G.P.D.P.; 1000 Genome Project Data Processing Subgroup. (2009). The Sequence Alignment/Map format and SAMtools. Bioinformatics *25*, 2078–2079.

Liu, L., Sabo, A., Neale, B.M., Nagaswamy, U., Stevens, C., Lim, E., Bodea, C.A., Muzny, D., Reid, J.G., Banks, E., et al. (2013). Analysis of rare, exonic variation amongst subjects with autism spectrum disorders and population controls. PLoS Genet. *9*, e1003443.

Malhotra, D., and Sebat, J. (2012). CNVs: harbingers of a rare variant revolution in psychiatric genetics. Cell *148*, 1223–1241.

Neale, B.M., Kou, Y., Liu, L., Ma'ayan, A., Samocha, K.E., Sabo, A., Lin, C.F., Stevens, C., Wang, L.S., Makarov, V., et al. (2012). Patterns and rates of exonic de novo mutations in autism spectrum disorders. Nature *485*, 242–245.

O'Roak, B.J., Deriziotis, P., Lee, C., Vives, L., Schwartz, J.J., Girirajan, S., Karakoc, E., Mackenzie, A.P., Ng, S.B., Baker, C., et al. (2011). Exome sequencing in sporadic autism spectrum disorders identifies severe de novo mutations. Nat. Genet. *43*, 585–589.

O'Roak, B.J., Vives, L., Fu, W., Egertson, J.D., Stanaway, I.B., Phelps, I.G., Carvill, G., Kumar, A., Lee, C., Ankenman, K., et al. (2012a). Multiplex targeted sequencing identifies recurrently mutated genes in autism spectrum disorders. Science *338*, 1619–1622.

O'Roak, B.J., Vives, L., Girirajan, S., Karakoc, E., Krumm, N., Coe, B.P., Levy, R., Ko, A., Lee, C., Smith, J.D., et al. (2012b). Sporadic autism exomes reveal a highly interconnected protein network of de novo mutations. Nature *485*, 246–250.

Parikshak, N.N., Luo, R., Zhang, A., Won, H., Lowe, J.K., Chandran, V., Horvath, S., and Geschwind, D.H. (2013). Integrative functional genomic analyses implicate specific molecular pathways and circuits in autism. Cell *155*, this issue, 1008–1021.

Sanders, S.J., Ercan-Sencicek, A.G., Hus, V., Luo, R., Murtha, M.T., Moreno-De-Luca, D., Chu, S.H., Moreau, M.P., Gupta, A.R., Thomson, S.A., et al. (2011). Multiple recurrent de novo CNVs, including duplications of the 7q11.23 Williams syndrome region, are strongly associated with autism. Neuron *70*, 863–885.

Sanders, S.J., Murtha, M.T., Gupta, A.R., Murdoch, J.D., Raubeson, M.J., Willsey, A.J., Ercan-Sencicek, A.G., DiLullo, N.M., Parikshak, N.N., Stein, J.L., et al. (2012). De novo mutations revealed by whole-exome sequencing are strongly associated with autism. Nature *485*, 237–241.

Schmidt, E.F., Kus, L., Gong, S., and Heintz, N. (2013). BAC transgenic mice and the GENSAT database of engineered mouse strains. Cold Spring Harb. Protoc. *2013*, pdb.top073692.

Sebat, J., Lakshmi, B., Malhotra, D., Troge, J., Lese-Martin, C., Walsh, T., Yamrom, B., Yoon, S., Krasnitz, A., Kendall, J., et al. (2007). Strong association of de novo copy number mutations with autism. Science *316*, 445–449.

State, M.W., and Levitt, P. (2011). The conundrums of understanding genetic risks for autism spectrum disorders. Nat. Neurosci. *14*, 1499–1506.

State, M.W., and Sestan, N. (2012). Neuroscience. The emerging biology of autism spectrum disorders. Science *337*, 1301–1303.

Workman, A.D., Charvet, C.J., Clancy, B., Darlington, R.B., and Finlay, B.L. (2013). Modeling transformations of neurodevelopmental sequences across mammalian species. J. Neurosci. *33*, 7368–7383.

EXTENDED EXPERIMENTAL PROCEDURES

Exome Data and Mutations
Published De Novo Mutations

Published de novo variants detected by exome sequencing in 943 ASD probands were obtained from the supplemental data of four publications: 225 from the Simons Simplex Collection (SSC) (Sanders et al., 2012), 343 from the SSC (Iossifov et al., 2012), 200 from the SSC (O'Roak et al., 2012b), and 175 from the ARRA consortium (Neale et al., 2012).

In addition de novo variants detected by exome sequencing in 543 matched siblings of ASD probands were obtained from the supplemental data of two publications: 200 from the SSC (Sanders et al., 2012) and 343 from the SSC (Iossifov et al., 2012).

To maximize our detection of de novo loss of function mutations we included two further papers: 1) genome-wide sequencing of 44 probands with ASD (Kong et al., 2012) in which two de novo loss of function (LoF) mutations were described; and 2) targeted sequencing of genes with known de novo variants (O'Roak et al., 2012a). To keep the analysis consistent only mutations in samples already sequenced using exome technology were included. These two publications added two further 2-hit hcASD genes, which were used as seeds: *CUL3* (Kong et al., 2012) and *TBR1* (O'Roak et al., 2012a). All de novo variants from all studies were re-annotated according to the Consensus CDS database (Harte et al., 2012; Pruitt et al., 2007).

The total samples size of published data is therefore 987 probands, 543 of which have de novo data for matched siblings.

Additional Exome Samples from 56 Families

Whole-blood derived DNA for 56 families chosen at random from the Simons Simplex Collection was subjected to exon capture using the Nimblegen EZ Exome V2.0 array and sequenced with 74bp paired-end reads on the Illumina HiSeq 2000. Sequence reads were aligned to hg19 using BWA (Li and Durbin, 2009); duplicate reads were removed with Samtools (Li et al., 2009). Single nucleotide variants were predicted using Samtools (Li et al., 2009) and de novo variants were identified using in-house scripts (Sanders et al., 2012). All de novo variants were confirmed using PCR and Sanger sequencing. Complete details of our methods for sequencing and analyzing de novo variants can be seen in our previous publication (Sanders et al., 2012). Details of the 56 additional SSC families are shown in Table S1.

Detection of Insertion-Deletions

To maximize our detection of de novo loss of function variants we reassessed 225 trios from our previous publication (Sanders et al., 2012) to detect de novo frameshift insertion-deletions (indels). The aligned BAM files were analyzed using local realignment with dindel (Albers et al., 2011). Ten further de novo frameshift indels were detected and confirmed using PCR and Sanger sequencing.

Confirmation of De Novo Events

The rarity of de novo variants increases the potential for false positive variants in the children and false negatives in the parents. The vast majority of de novo LoF variants used as the input for the analyses presented in the main manuscript have been confirmed through PCR of the interval in the child and both parents, followed by Sanger sequencing to demonstrate that a variant is present and that it is truly de novo. Out of 144 de novo LoF variants in this analysis, 138 (96%) have been confirmed. Of the remaining six variants, five are de novo frameshift indels from the Iossifov paper (*MED13L*, *BCL11A*, *EFCAB5*, *TRIM17*, *TROVE2*) in which confirmation has not been reported however, they do demonstrate a 96% (148/154) de novo confirmation rate for the de novo variants for which confirmation was reported. The final de novo LoF that is not explicitly confirmed is *CUL3* from the Kong paper; they demonstrate a 99% (93/94) de novo confirmation rate; however, it is not stated whether this de novo LoF mutation was included within this set.

De Novo Mutation Burden

The combination of published and new exome data yields a total data set of 1,043 probands and 599 matched unaffected siblings. To estimate the significance of observing multiple de novo variants in the same gene it was necessary to estimate the odds ratio between matched probands and siblings. The results for 599 matched probands and siblings are shown in Figure S1. The de novo variants used for this analysis are shown in the tab marked "Burden_LoF" in Table S1. The odds ratio for de novo LoF mutations was 2.21 (95%CI: 1.45-3.36; $p = 5 \times 10^{-5}$, binomial exact test). Considering all the 1,043 ASD samples we obtained a list of 144 de novo LoF mutations, these are shown in the tabs marked "hcASD" and "pASD" in Table S1.

Significance of Multiple De Novo LoF Mutations in the Same Gene

To estimate the significance of observing multiple de novo LoF mutations in the same gene for probands we need to estimate the chance of observing this outcome for the non-ASD associated de novo LoF mutations in siblings. In 1,043 ASD probands we observed 144 de novo LoF mutations. Based on the observed odds ratio of 2.21 we would expect 63 de novo LoF mutations in siblings. From this number we can estimate the probability of seeing 2 de novo LoF mutations in the same gene under the null hypothesis (a 2-hit gene).

p value. Based on the birthday problem logic we can estimate the chance of observing 2 out of 63 LoF mutations in the same gene out of the 18,933 possible RefSeq genes as being 0.10 (this is the genome-wide p value for a 2-hit gene and also the number of expected 2-hit genes). However genes differ in size and GC content, both of which are associated with more de novo mutations. A permutation test based on the 18,933 RefSeq genes was performed to allow size and GC content to be taken into account and the p value was revised upward to 0.1975.

q value. The p value assesses the chance of observing a 2-hit gene at least once in the experiment. The q-value, or false discovery rate (FDR), assesses the chance of observing two hits in a specific gene. Based on the permutation test we expect to observe 0.1975 such genes; however, we observe 9 genes with at least two de novo LoF mutations. Each gene with two de novo mutations is 45.57

times more likely to be a true ASD gene than a random 2-hit gene (9/0.1975). The q-value/FDR is therefore 0.022 (1/45.57) meaning that each 2-hit gene is an ASD gene with 97.8% confidence (1 - 0.022 * 100).

Applying these same methods to a 3-hit gene (i.e., 3 or more de novo LoF mutations in the same gene) yields a p value of 0.0008 and a q-value of 0.0002 giving a confidence of 99.98% that such a gene is a true ASD gene and exceeding the threshold for being genome-wide significant. Likewise a 1-hit gene has a q-value of 0.45 and a 55% confidence of being a true ASD gene.

Based on these metrics we designated a gene as being a high-confidence ASD gene (hcASD) if there were 2 or more de novo LoF mutations; 9 genes met or exceeded this threshold: one previously unreported gene with two de novo LoF mutations: *Ankyrin 2, neuronal* (*ANK2*); and eight previously reported hcASD genes: four with three or more de novo LoF mutations – *Chromodomain helicase DNA binding protein 8 (CHD8); Dual-specificity tyrosine-(Y)-phosphorylation regulated kinase 1A (DYRK1A); Glutamate receptor, ionotropic, N-methyl D-aspartate 2B (GRIN2B);* and *Sodium channel, voltage-gated, type II, alpha subunit (SCN2A)*; and four with two de novo LoF mutations – *Cullin 3 (CUL3); Katanin p60 subunit A-like 2 (KATNAL2); Pogo transposable element with ZNF domain (POGZ);* and *T-box, brain, 1* (*TBR1*). A gene was designated as a probable ASD gene (pASD) if there was a single de novo LoF mutation; 122 genes met this criterion. A complete list of these genes and the de novo LoF mutations are shown in the tabs marked "hcASD" and "pASD" in Table S1.

Construction of Spatiotemporal Coexpression Networks

Gene level expression data (Platform GPL5175; Affymetrix GeneChip Human Exon 1.0 ST Array) were downloaded from the National Center for Biotechnology Information (NCBI) Gene Expression Omnibus (GEO accession number GSE25219) (Kang et al., 2011). Based on the quality control and quantile normalization by Kang et al. (2011) as well as their calculated gene-level expression values, expression data from the core probe set were used in coexpression analysis (exceptions: for hcASD gene *CHD8* and the pASD genes *FLG, FREM3, FRG2C, LMTK3, THSD7A, UBN2,* and *ZNF594*, data from the extended probe set were utilized). Genes with multiple transcript IDs (316 total) were removed from the analysis (exceptions: for *CHD8* and the pASD genes *FAM91A1, FREM3,* and *UBN2*, gene expression values from multiple transcript IDs were combined by averaging all data that mapped to the correct genomic locus). Specifically, for *CHD8* two of the three extended probe sets were averaged (transcript IDs 3520878 and 3528085 averaged, 3555882 excluded); for *FAM91A1* both core probe sets were averaged (transcript IDs 3114358 and 3114365); for *FREM3* all three extended probe sets were averaged (transcript IDs 2787812, 2787824, and 2787831); and for *UBN2* only one of the two extended probe sets was utilized (transcript ID 3026891 used, 3075658 excluded). Of note, only 116 of the 122 pASD genes had gene expression data (see Table S1) and so all pASD enrichment analyses were based on these 116 genes.

Coexpression analysis was conducted with an in-house R script. Briefly, within each postmortem brain, gene expression values were determined per region: multiple tissue samples within the same region (i.e., different hemispheres, etc) were averaged, resulting in a vector of expression values (expression profile) for each gene by brain region and brain sample. Within each spatiotemporal window, the vector of expression values was trimmed to relevant regions and brain samples only. Next, the Pearson correlation coefficient for the trimmed expression profile was calculated for each pairwise combination of genes. For each seed gene, the top 20 best correlated genes with an absolute correlation coefficient with the seed gene of $\geq$ 0.7 selected; each network is composed of the hcASD genes and their top correlated genes. Edges are then formed between any network gene with absolute correlation coefficient $\geq$ 0.7. Any hcASD genes without edges were removed.

Temporal windows were determined solely by taking overlapping sets of three consecutive periods of development, starting with periods 1-3 and ending at periods 13-15. This provided adequate numbers of data points, as well as sufficiently dynamic data in each window, to assess correlations of changes in gene expression robustly while still preserving temporal resolution. To determine spatial windows, coherent subsets of brain regions were grouped based on transcriptional similarity. The presence of a strong signal in period 3-5 and 4-6 in all brain and in the neocortex (Figure S2A) indicated clustering of brain regions by transcriptional similarity during fetal development would increase resolution of our network analysis by separating these regions meaningfully during this time. As well, gene expression changes are most dynamic during fetal development (Kang et al., 2011). Therefore, using expression data from fetal development (periods 3-7), within each brain region gene expression values were summarized by taking the median across all samples within the same brain specimen (expression values of probe sets targeting the same gene were averaged). Pairwise Spearman correlations between brain regions were then determined, and regions were hierarchically clustered in R using the "hclust" function (1 – corr^2 as the distance, clustering using Ward's method). Distinct clusters of brain regions informed spatial window construction (see main text Figure 2A). Specifically, within the developing neocortex, the prefrontal cortex (PFC) areas (MFC, OFC, DFC and VFC) formed a distinct cluster, while the frontal primary motor cortex (M1C) clustered with its topographic neighbor, the primary somatosensory area (S1C). The clustering of M1C and S1C is at least in part driven by the fact that the two areas cannot be reliably distinguished until late midfetal development, due to the absence of the central sulcus. Together, the PFC, M1C, and S1C areas formed a separate larger cluster herein collectively referred to as the PFC-MSC (prefrontal cortex and primary motor-somatosensory cortex), which is clearly distinguishable from another large cluster comprised of the posterior perisylvian areas (IPC, STC, and A1C) and ITC, while the V1C was the most transcriptionally divergent among all analyzed neocortical areas.

Permutation Tests

In the main manuscript we describe how spatiotemporal coexpression networks built around 9 hcASD seed genes (each with > 97% confidence for being an ASD gene) can be assessed for enrichment of pASD genes (each with 55% confidence for being an ASD

gene). The enrichment of pASD genes was observed in four specific brain regions and time periods: period 3-5 PFC-MSC, period 4-6 PFC-MSC, period 7-9 V1C-STC, and period 8-10 MD-CBC (Figure 2). The analysis was performed using a hypergeometric test (Figure 2), which makes the assumption that there is an equal chance of a pASD gene and a non-pASD gene being included in the network. However de novo mutations are more frequent in larger genes, effectively reducing the number of genes likely to contain a mutation and potentially leading to liberal estimates of p values. As well, network structure (i.e., correlations between genes) may also confound estimates.

To obtain a measure of significance that better reflects the subtleties of coexpression data we used a permutation test based on selecting 9 pseudo-hcASD seed genes, based on the likelihood of observing 2-hit de novo LoF mutations by chance (taking gene size and GC content into account; Sanders et al., 2012). Coexpression networks were built around each set of 9 pseudo-hcASD genes using the period 3-5 PFC-MSC, period 4-6 PFC-MSC, period 7-9 V1C-STC, or period 8-10 MD-CBC data. By assessing enrichment for pASD this analysis demonstrated a significant result for both midfetal modules as well as the period 8-10 MD-CBC network, but not for the period 7-9 V1C-STC network (100,000 iterations). Of note, for this and all downstream analyses that evaluate multiple hypotheses (e.g., multiple stages of development and/or regions of the brain), p values are corrected for multiple comparisons by using the conservative Bonferroni correction within a family of tests.

Permuting pASD Genes
The above permutation analysis tests the hypothesis that the identification of the 9 hcASD genes is critical to detection of the pattern of spatiotemporal pASD enrichment that we observed. To further confirm the robustness of our findings we considered the hypothesis that the identification of the 122 pASD genes was also critical to the detection of spatiotemporal enrichment. To test this we performed a permutation test in which the 9 hcASD genes remained constant while the 116 pASD genes with expression data were selected based on the likelihood of observing 1-hit de novo LoF mutations by chance (taking gene size and GC content into account and excluding the 9 seed genes from the list of possible genes; Sanders et al., 2012). This permutation test was run to 100,000 iterations on each of the three spatiotemporal networks showing de novo LoF enrichment: period 3-5 PFC-SMC (p < 0.001, corrected for 91 comparisons); period 4-6 PFC-SMC (p = 0.01, corrected for 91 comparisons); period 8-10 CBC-MD (p = 0.009, corrected for 91 comparisons); these results are shown in Figure S2D. The 100,000 iterations were insufficient to detect a single iteration of 11 or 12 permuted pASD genes in the network therefore the results were extrapolated from the data from 0 to 10 permuted pASD genes to estimate the p value.

Permuting Number of Coexpressed Genes
Given the reliance on a bottom-up approach (i.e., building networks around a few high confidence genes as opposed to a top-down approach in which all genes are used to make a network which is then split into modules e.g., WGCNA) we considered how robust our results were to varying the number of coexpressed genes that were selected for each seed gene. In the main manuscript we used the 20 most highly correlated (Pearson's correlation) genes for each seed gene. To test this we used the same permutation test described in the main manuscript (permuting the 9 hcASD seed genes) but varied the number of most highly correlated genes selected for each seed between 5 and 500. For each number of most highly correlated genes 1,000 permutations were performed. The results show a great deal of stability with 10-300 genes exceeding a significance threshold of 0.05 for period 3-5 PFC-SMC and 5-90 genes exceeding the same threshold for period 4-6 PFC-SMC (Figure S2E).

Permutation Tests for Enrichment of Other Genes
The 100,000 networks built around 9 pseudo-hcASD genes (see Permutation Tests above) for period 3-5 PFC-MSC, and the further 100,000 networks for period 4-6 PFC-MSC and for period 8-10 MD-CBC, were used as the basis for other permutation-based downstream analyses including TADA enrichment, connectivity, layer specific marker genes and cell-type specific marker genes. In each case, we compared the observed enrichment to the distribution of enrichment in the permuted networks.

Cross-validation Experiment
To test further the robustness of our findings, we performed a cross-validation experiment with 200 iterations: for each iteration we randomly removed one hcASD seed gene and 10% (12) of the pASD genes, constructed all 52 spatiotemporal coexpression networks, and assessed the number of remaining pASD genes found within each network. We assessed the number of times that one or more of the top three networks (PFC-MSC in period 3-5 and 4-6, and MD-CBC in period 8-10; Figure 2B) was the most enriched for pASD genes. Consistent with our initial findings, we observed this 100% of the time (Table S2), suggesting the observed spatiotemporal localization is robust to the set of input genes.

Single Period Weighted Analysis
Finally, to ensure that the observed temporal and spatial localization was not an artifact of the choice of three period sliding windows ("windowed" analysis), we conducted a complementary single period "weighted" analysis approach that places the greatest emphasis on individual periods while including data from the prior and subsequent interval. Specifically, for each network, the coexpression data for the period is given a weight of 1 and the periods immediately before and after are given a weight of 0.5. Using this method, we observed essentially identical results in terms of temporal and spatial specificity (Figure S2C).

Transmission and De Novo Association Test
Comparison of the burden of de novo LoF mutations detected by whole-exome sequencing (WES) in probands and their matched unaffected siblings shows that a gene with a single proband de novo LoF mutation has a 55% chance of being a true ASD risk

gene. By considering further information about the gene's characteristics and other potential risk variants it is possible to refine this 55% estimate on a per-gene basis. He et al. (2013) developed the transmission and de novo association (TADA) test to integrate WES data from family and case-control studies alongside estimates of gene mutability based on gene size and GC content. TADA has been validated theoretically and by simulations of data on rare, large-effect mutations affecting risk for ASD. TADA p values from He et al. (2013) were updated with the additional de novo and inherited variant data from the additional 56 quartets sequenced as part of this study. These updated p values were utilized in the TADA permutation test.

Period 8–10 MD-CBC Network

The period 8-10 MD-CBC network was significantly enriched for pASD genes (9/116 pASD genes, corrected p = 3.5x10^{-4} by hypergeometric test, corrected p = 0.04 by permutation test), but there are relatively few samples underlying this result: 26 compared to 107 and 140 in the period 3-5 and period 4-6 networks, respectively. Thus, the remainder of the analyses in the main text focused on the networks from period 3-5 and 4-6 in the PFC-MSC cluster. However, we did assess several metrics of this network including, connectivity, and TADA enrichment by the same permutation test used in the main text.

Figure S3A summarizes the period 8-10 MD-CBC network. Visually, this network does not appear highly connected in comparison to the two midfetal networks. While significant enrichment of pASD is observed by hypergeometric test and the more stringent permutation test, the connectivity of this network is not significantly enriched (p = 0.80) in contrast to the period 3-5 (p = 0.03) and period 4-6 (p = 0.02) networks. Finally, like the two midfetal networks, the set of pASD genes present in the network is enriched for pASD genes with a high probability of association with ASD based on TADA (p = 0.01, Figure S3B). However, this result is two orders of magnitude less significant than the corresponding scores for the two midfetal networks (Figures 3C and 3D).

TBR1 KO mRNA-Seq and Data Analysis

Total RNA was isolated from freshly dissected postnatal day 0 (P0, equivalent to human early midfetal development; Workman et al., 2013) neocortices of $Tbr1^{-/-}$ and $Tbr1^{+/+}$ littermates using a QIAGEN RNeasy Mini Kit. Libraries were prepared using an Illumina mRNA-Seq Sample Prep Kit. Amplified cDNA was size-selected at 250 bp and validated using the Agilent Bioanalyzer DNA 1000 system. The final product was subjected to cluster generation using an Illumina Standard Cluster Generation Kit v4. Libraries were sequenced as single end 74mers using the Illumina Genome Analyzer pipeline, and image analysis (Firecrest module), base-calling (Bustard module), and primary sequence analysis (Gerald module) were performed. Reads were mapped to the mouse reference genome (release mm9) with ELAND software. Filtered reads that were uniquely mapped to exons of Ensembl gene model with up to two mismatches were used for the quantification of gene expression. To detect differentially expressed genes between $Tbr1-/-$ and $Tbr1+/+$, we designed a three-step stringent filtering process. First, counts of mapped reads within genes were compared using Fisher's exact test (adjusted p $\leq$ 0.05). Second, reads per kb of exon model per million reads (RPKM = 10^9 C/NL, where C is the number of mappable reads that fall onto the gene's exons, N is the total number of mappable reads in the lane, and L is the sum of the exons in base pairs) were used to quantify gene expression, and the fold change was set as another filtering scale (|log2(fold change)| $\geq$ 0.5). In our series of relative experiments, the genes were finally identified as differentially expressed unless they were shared by all groups.

Animals

All experiments were carried out in accordance with a protocol approved by the Committee on Animal Research at Yale University. $Tbr1$ mutant mice were a generous gift from John Rubenstein. The generation of $Tbr1^{-/-}$ allele was described previously (Bulfone et al., 1998).

Network Analysis with Human Laminar-Specific Expression Data

Region and layer specific gene expression data were obtained from the BrainSpan Prenatal LMD Microarray project. This data set profiles gene expression in four brains spanning periods 4 to 6 of development (15-21 postconceptual weeks). In each brain, gene expression profiles were assessed for 347 finely laser microdissected tissue samples from subdivisions distributed across cortical and noncortical regions. For more information on data generation, please see the corresponding technical white paper on the project website (http://www.brainspan.org/).

In order to test laminar location of the two midfetal prefrontal and primary motor-somatosensory cortex (PFC-MSC) networks we assumed they were localized to the brain regions contained within the PFC-MSC area, and therefore, utilized expression data from the LMD microarray corresponding to these anatomical regions only (dorsolateral and ventrolateral prefrontal, orbital frontal, posterior frontal (motor), frontal pole, and primary somatosensory cortical regions). Within each of these regions samples from nine layers were assessed: subpial granular zone, marginal zone, outer cortical plate, inner cortical plate, subplate zone, intermediate zone, outer subventricular zone, inner subventricular zone, and ventricular zone (listed from cortical to ventricular surface).

To assess the relevance of the two networks to each of the nine layers, we recreated the original networks within each layer (based on expression data from samples collected within that layer only) and then assessed their connectivity. More specifically, we determined Pearson's correlation coefficients between network genes connected in the original midfetal networks, using expression data from each layer separately. By summing these correlations, we were able to estimate the overall connectivity of the networks layer-by-layer, and then to assess the significance of this connectedness using a permutation test with 100,000.

We calculated normed correlations in order to remove biases that have to do with global changes in connectivity:

Let i and j denote genes and k denote layer. Define r_{ijk} as the correlation between genes i and j in layer k, and define $\bar{r}_k$ as the average correlation, over all pairs of the genes measured in layer k. Then define a normed correlation as

$$c_{ijk} = \frac{r_{ijk}}{\bar{r}_k}.$$

Connectivity of a network in layer k was then calculated by summing c_{ijk} for all pairs in the network.

For each iteration of the permutation test, the 2,952 and 3,389 gene-gene correlations from the original period 3-5 and 4-6 networks, respectively, were kept constant; however, the normed correlation value between each of the pairs of genes within a network was chosen randomly from one of the 9 layers for each gene. In other words, we permuted the (i,j) connections over the set of k 100,000 times in order to get the null distribution of connectivity. This approach was chosen in order to simulate the set of possible sums of a network not enriched in a specific layer.

For subdivision and analysis of the two subnetworks in the period 3-5 PFC-MSC network, we visually separated the whole network into two subnetworks (*ANK2-CHD8-CUL3-DYRK1A-SCN2A-TBR1* and *POGZ-GRIN2B*; corresponding genes are in Table S3). We then performed the same connectivity analysis described above for both sub-networks but using the smaller pool of within subnetwork connections.

Enrichment Analysis in Mouse Neocortical Layers across Development

Different layers of the mouse cerebral neocortex were microdissected from live tissue sections of the *Dcdc2a*-GFP transgenic reporter mouse (obtained from the GENSAT project; Schmidt et al., 2013), which expresses GFP selectively in L4 pyramidal and stellate glutamatergic excitatory neurons. Tissue samples were collected from the primary somatosensory area (e.g., equivalent to human SC1 area) of mice brain at postnatal days 4 (P4), P6, P8, P10, P14, and adult (P180 or six months old mice). Based on a mathematical model to translate neurodevelopmental time across mammals (http://www.translatingtime.net; Workman et al., 2013), a brain growth event in the cortex of the mouse at P4 [postconception (PC) day 22.5] translates to PC day 159, or approximately to the middle of period 6, in the human. Mouse P6 (PC 24.5), P8 (PC 26.5), P10 (PC 28.5), P14 (PC 32.5) and P180 (PC 198.5), translate to PC day 188 (early period 7), 219 (middle period 7), 253 (late period 7), 328 (early period 8), and young adult (period 13), respectively.

We assumed that each layer contains multiple but also unique cell types with identifiable and divergent gene expression profiles that allow us to follow the molecular dynamics of different neuronal and glial populations. For example, the DL are composed by the first born glutamatergic excitatory projection (pyramidal) neurons to arrive to the developing cortical plate, which project axons mainly to subcortical regions. On the other hand, UL are composed by the last borne glutamatergic excitatory projection (pyramidal) neurons to arrive to the developing cortical plate, which for the most part project intracortically (also known as corticocortical projections). Lastly, L4 is generally composed by two groups of glutamatergic excitatory neurons: smaller size pyramidal neurons, and spiny stellate cells (also known as granule cells), which specifically within the sensory cortices establish local synaptic connections with neighboring cells.

Details on the microdissection and RNA-seq will be published separately. Briefly, the microdissection of the superficial layers (SL) (i.e., L2/3 including marginal zone or L1, and pia), L4, and deep layers (DL) (i.e., L5/6 including transient subplate zone or adult white matter) was performed on 250 mm thick slices, while maintaining the section submerged in ice-cold ACSF inside a petri dish, using a scalpel and a dissecting needle, under a fluorescence stereoscope (Discovery V8, Zeiss). Total RNA was extracted from each sample (e.g., SL, L4, and DL). The cDNA libraries were prepared using the TruSeq mRNA Sample Prep Kit (Illumina) as per the manufacturer's instructions with some modifications. Briefly, polyA RNA was purified from 1 μg of total RNA using oligo(dT) beads. Quaint-IT RiboGreen RNA Assay Kit (Invitrogen) was used to quantitate purified mRNA with the NanoDrop 3300 (Thermo Scientific). The denatured libraries were diluted to 15 pM, followed by cluster generation on a single-end HiSeq flow cell (v1.5) using an Illumina cBOT, according to the manufacturer's instructions. The HiSeq flow cell was run for 75 cycles using a single-read recipe (v2 sequencing kit) according to the manufacturer's instructions.

Reads passing the default purify filtering of Illumina CASAVA pipeline (released version 1.7) were aligned to mouse reference genome (GRCm38/mm10) using Tophat 2.0.8 (Kim et al., 2013; Kim and Salzberg, 2011; Langmead et al., 2009; Trapnell et al., 2009). Full-length reads were used (75 bp). The Cufflinks 2.1.1 program Cuffdiff (Trapnell et al., 2012) identified differentially expressed genes using the mm10 annotation from UCSC. The two mice at each time point were treated as biological replicates.

At each time point (P4, P6, P8, P10, P14, and P180) genes exclusively upregulated in each layer were identified by the following criteria: FPKM $\geq$ 10, and for both comparisons with the other two layers, a q-value (FDR) $\leq$ 0.05, and fold change $\geq$ 2. The stringent threshold of FPKM $\geq$ 10 was used to identify differentially expressed genes more likely to be important to layer identity.

Genes exclusively upregulated in each layer at each time point were termed marker genes for that layer and time. We then assessed enrichment of the set of markers for each layer and time point using the hypergeometric distribution function "phyper" in R. At each time point, q = number of marker genes in network; m = total number of marker genes; n = the difference between the number of genes with status "ok", expression level in at least one layer $\geq$ 10 FPKM, and a human ortholog, and m; and k = the number of genes in the network.

In this and all downstream analyses, an in-house database of mouse and human orthologs converted mouse genes to human genes in order to assess enrichment in the networks built with human genes.

Cell-Type-Specific Markers

Cell-type specific marker genes were derived from a previously published and independent list derived from human expression data (Kang et al., 2011). Kang et al. (2011) assessed the BrainSpan exon array developmental transcriptome and determined markers of five cell types: astrocytes, cortical GABA interneurons, cortical glutamatergic neurons, microglia, and oligodendrocytes (Table S6). After observation of significant enrichment of cortical glutamatergic projection neuron (CPN) marker genes only, enrichment of marker genes specific to layer (L) 5/6 CPNs and to L1-4 CPNs (Table S6) was determined. The significance of the observed enrichment for a particular cell type was calculated by assessing the test set of 100,000 networks for the distribution of marker gene enrichment.

Immunostaining and In Situ Hybridization

Coronal sections from 17-20 PCW human frontal cortex were used to validate the cellular resolution of ASD gene expression. For immunohistochemistry, sections were pretreated with 0.3% H_2O_2 followed by incubation in blocking buffer at room temperature and then incubation for 24-48 hr at 4°C in primary antibodies. Tissue was then incubated with biotin-labeled secondary antibodies, conjugated with Avidin-Biotin-Peroxidase Complex (Vector Laboratories), and visualized with DAB (Vector Laboratories) following the manufacturer's recommended protocol. Antibodies used were: rabbit anti-TBR1 (1:250, Abcam); rabbit anti-POGZ (1:250, Sigma-Aldrich); rabbit anti-CHD8 (1:500, Novus); and biotin-conjugated donkey anti-rabbit (1:200, Jackson ImmunoResearch). Developed sections were mounted on Superfrost Plus charged slides (Fisher), dehydrated through an ethanol series, cleared with xylenes, and preserved with Permount (Fisher) and glass coverslips. Images were taken using a digital scanner (Aperio ScanScope).

Immunofluorescent staining was performed similarly as aforementioned, without peroxide pretreatment, and with longer incubations in blocking buffer, primary and secondary antibodies, and intermittent washes. Additional antibodies used were goat anti-FOXP2 (1:200, Santa Cruz); mouse anti-SATB2 (1:200, GenWay); and flurophore-conjugated secondary antibodies (AlexaFluor from Life Technologies). DAPI was included during incubation with secondary antibodies to counterstain nuclei. After staining, sections were mounted as before and preserved with Aqua Poly/Mount (Polysciences) and glass coverslips.

For in situ hybridization, brain sections were first mounted on charged slides, followed by postfixation in 4% paraformaldehyde-PBS and then a 0.1 M triethanolamine with 0.25% acetic anhydride pretreatment. Sections were then incubated overnight at 65°C with 500 ng/ml of digoxigenin (DIG)-labeled cRNA probes corresponding to human *SCN2A* nucleotides 1817-2954 (NM_001040143). Sections were washed and incubated overnight at 4°C with alkaline phosphatase-conjugated anti-DIG antibodies, followed by signal detection using NBT/BCIP chromogen (Roche) diluted in a PVA buffer. Tissue was again postfixed in paraformaldehyde, then dehydrated and coverslipped as for the DAB-stained sections.

SUPPLEMENTAL REFERENCES

Bulfone, A., Wang, F., Hevner, R., Anderson, S., Cutforth, T., Chen, S., Meneses, J., Pedersen, R., Axel, R., and Rubenstein, J.L. (1998). An olfactory sensory map develops in the absence of normal projection neurons or GABAergic interneurons. Neuron *21*, 1273–1282.

Harte, R.A., Farrell, C.M., Loveland, J.E., Suner, M.-M., Wilming, L., Aken, B., Barrell, D., Frankish, A., Wallin, C., Searle, S., et al. (2012). Tracking and coordinating an international curation effort for the CCDS Project. Database (Oxford) *2012*, bas008.

Kim, D., and Salzberg, S.L. (2011). TopHat-Fusion: an algorithm for discovery of novel fusion transcripts. Genome Biol. *12*, R72.

Kim, D., Pertea, G., Trapnell, C., Pimentel, H., Kelley, R., and Salzberg, S.L. (2013). TopHat2: accurate alignment of transcriptomes in the presence of insertions, deletions and gene fusions. Genome Biol. *14*, R36.

Langmead, B., Trapnell, C., Pop, M., and Salzberg, S.L. (2009). Ultrafast and memory-efficient alignment of short DNA sequences to the human genome. Genome Biol. *10*, R25.

Pruitt, K.D., Tatusova, T., and Maglott, D.R. (2007). NCBI reference sequences (RefSeq): a curated non-redundant sequence database of genomes, transcripts and proteins. Nucleic Acids Res. *35*(Database issue), D61–D65.

Trapnell, C., Pachter, L., and Salzberg, S.L. (2009). TopHat: discovering splice junctions with RNA-Seq. Bioinformatics *25*, 1105–1111.

Trapnell, C., Roberts, A., Goff, L., Pertea, G., Kim, D., Kelley, D.R., Pimentel, H., Salzberg, S.L., Rinn, J.L., and Pachter, L. (2012). Differential gene and transcript expression analysis of RNA-seq experiments with TopHat and Cufflinks. Nat. Protoc. *7*, 562–578.
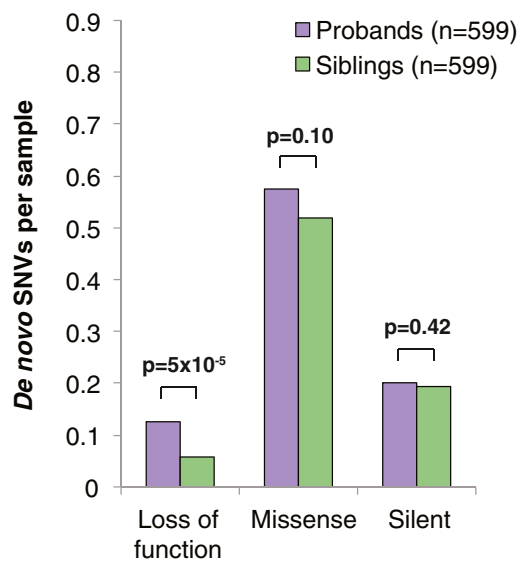
Figure S1. De Novo Burden Analysis, Related to Figure 1

The number of de novo mutations per sample are shown in 599 probands (purple) and 599 matched unaffected siblings (green) from the Simons Simplex Collection (SSC).
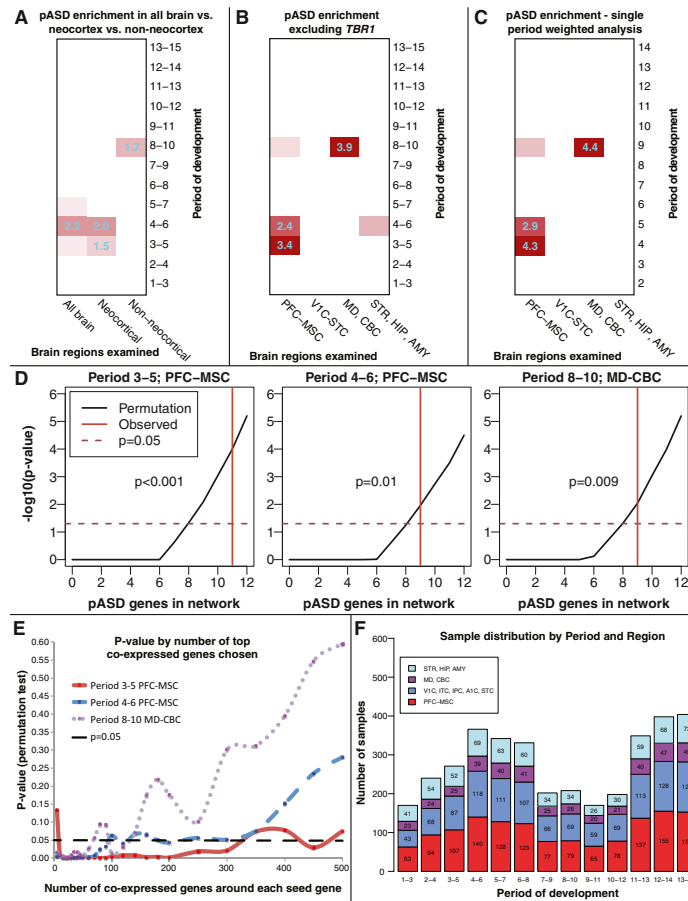
Figure S2. Additional Spatiotemporal Network Analyses and Permutation Tests, Related to Figure 2

(A) Networks built from all brain regions, neocortical regions, and nonneocortical regions. To achieve spatiotemporal resolution, coexpression networks were formed from subsets of the expression data based on developmental stage (in 3-period windows) and brain region. Each of the networks was tested for enrichment of 122 pASD genes. This heatmap shows the negative log$_{10}$(p value) of this enrichment (hypergeometric test) for each network with developmental stages on the y axis and brain regions on the x axis. Networks that are not significant are in white; nominally significant networks are in light red; networks that are significant after correction for multiple comparisons are in red and have the negative log$_{10}$(p value) overlaid with cyan text. The presence of a strong signal in period 3-5 and 4-6 in all brain and in the neocortex indicated clustering of brain regions by transcriptional similarity during fetal development (periods 3-7) would increase resolution of our network analysis by separating these regions meaningfully during this time. As well, gene expression changes are most dynamic during fetal development (Kang et al., 2011).

(B) The analysis in main text Figure 2 was repeated without *TBR1* as an hcASD gene. Excluding *TBR1* produces essentially identical results in terms of temporal and spatial specificity.

(C) The analysis in main text Figure 2 was repeated using a single period weighted approach that places the greatest emphasis on individual periods while including data from the prior and subsequent interval. Specifically, for each network, the coexpression data for the period is given a weight of 1 and the periods immediately before and after are given a weight of 0.5. This method shows essentially identical results in terms of temporal and spatial specificity as the three period sliding window analysis in Figure 2.

(D) Permutation test to estimate the significance of observing enrichment of multiple pASD genes in a coexpression network built around nine hcASD seeds by permuting the pASD genes. The black line shows the estimated p value as the number of pASD genes in the coexpression network increases (corrected for multiple comparisons); the vertical red line shows the number of pASD genes observed for each specific network. The dashed purple horizontal line represents the point on the y axis at which p = 0.05.

(E) The coexpression networks were built from the top 20 coexpressed genes for each seed gene. To assess whether the results were robust to altering the choice of 20 genes a permutation test was performed in which this number was varied between 5 and 500. The red, blue and purple lines show how the p value varied for the period 3-5 PFC-MSC, period 4-6 PFC-MSC, and period 8-10 MD-CBC respectively. The horizontal dashed black line represents the threshold of p = 0.05. All three networks were robust (below p = 0.05) to variation between 10 and 60 top coexpressed genes with the period 3-5 PFC-SMC network remaining significant up to 300 genes.

(F) The number of tissue samples available in the BrainSpan exon array data set for each spatiotemporal window is plotted by developmental window (x axis) and group of brain regions (colors). The total BrainSpan data set in Kang et al. (2011) comprises 1,340 tissue samples from 57 clinically unremarkable brain samples; however, the total number of samples listed in this figure is greater because the developmental windows are overlapping.
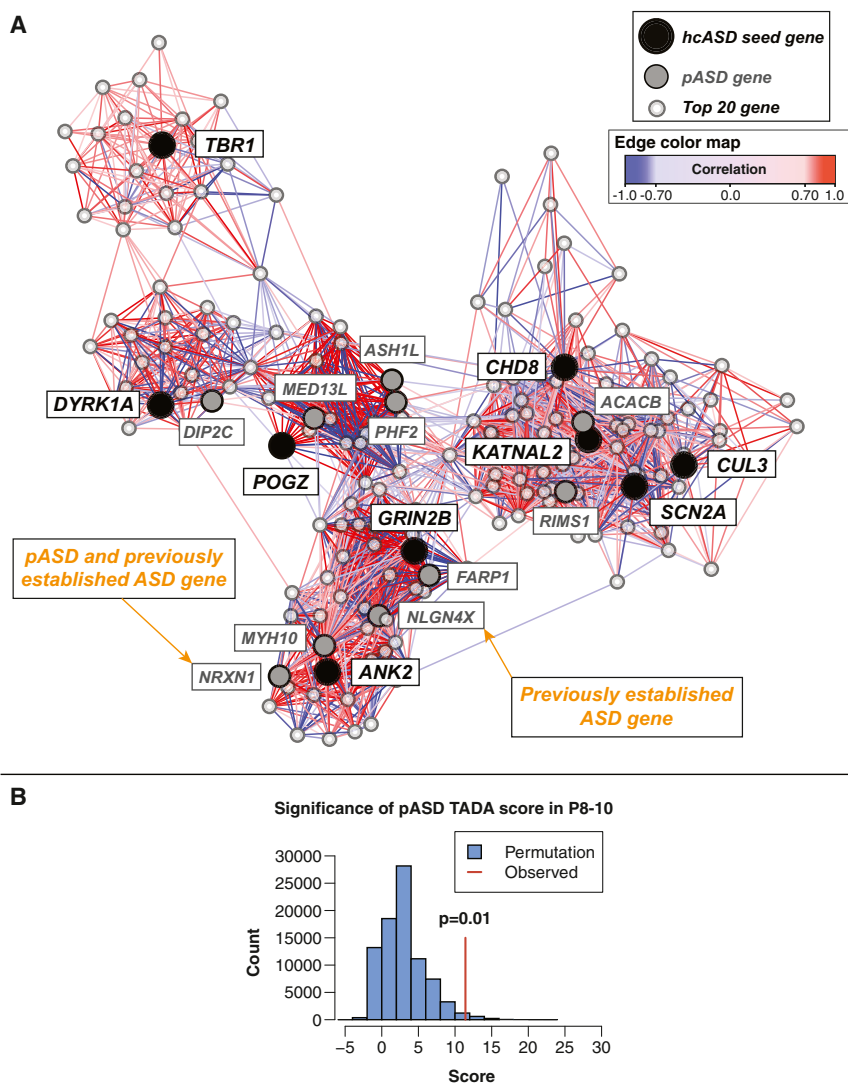
Figure S3. The Period 8–10 MD-CBC Network, Related to Figure 3

(A) The period 8-10 MD-CBC coexpression network. Gene coexpression analysis identified the 20 genes best correlated with each hcASD gene. The hcASD seed genes are in black; pASD genes identified within the network are in gray; and top 20 coexpressed genes that are not pASD genes are in white. The lines (edges) link genes with coexpression correlation > 0.7 and the shade represents the strength of the correlation; positive correlations are in in red; negative correlations are in blue. Previously established ASD genes *NLGN4X* and *NRXN1* (also a pASD gene) are highlighted with orange arrows.

(B) The TADA score uses inherited and mutation probability for each gene to assess which pASD genes are likely to be true ASD genes (He et al., 2013). This histogram shows the results of a permutation test (100,000 iterations) assessing the combined TADA score in the period 8-10 network; the observed score (11.4) is shown by the vertical red line and corresponds to a p value of 0.01.
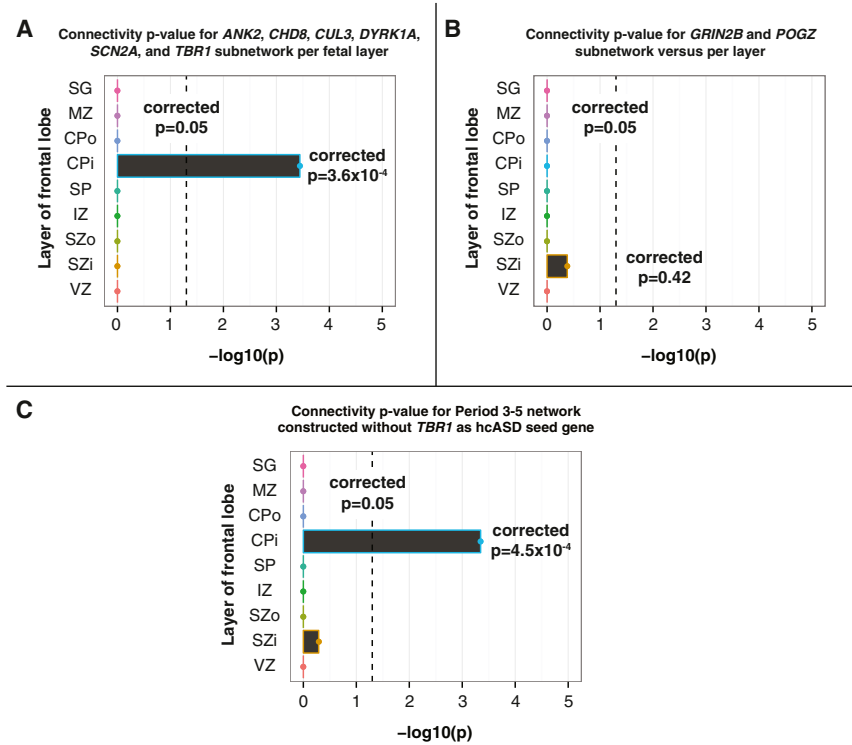
A

Connectivity p-value for *ANK2*, *CHD8*, *CUL3*, *DYRK1A*, *SCN2A*, and *TBR1* subnetwork per fetal layer

corrected p=0.05

corrected p=3.6x10^{-4}

B

Connectivity p-value for *GRIN2B* and *POGZ* subnetwork versus per layer

corrected p=0.05

corrected p=0.42

C

Connectivity p-value for Period 3-5 network constructed without *TBR1* as hcASD seed gene

corrected p=0.05

corrected p=4.5x10^{-4}

Figure S4. Additional Layer-Specific Analyses, Related to Figure 4

The connectivity of two subnetworks within the period 3-5 network were assessed in a separate prenatal transcriptome (BrainSpan, www.brainspan.org). This data set is comprised of microarray-based gene expression profiles of laser micro-dissected human midfetal (period 4-6) brains. Significance of the observed extent of connectivity (sum of correlations along network connections) for each layer was assessed by permutation test.

(A) The *ANK2*, *CHD8*, *CUL3*, *DYRK1A*, *SCN2A*, and *TBR1* subnetwork shows greatest connectivity in the CPi region (inner cortical plate) corresponding to neocortical layers 5-6 (corrected p = 3.6x10^{-4}).

(B) The *GRIN2B* and *POGZ* subnetwork shows greatest connectivity in the VZ region (corrected p = 0.42).

(C) The connectivity of the period 3-5 network built excluding *TBR1* (see Figure S2) was assessed as in 'A' and 'B'. This network shows greatest connectivity in the CPi region (corrected p = 4.5x10^{-4}), and therefore, excluding *TBR1* produces essentially identical results with respect to laminar specificity as the three period sliding window analysis in main text Figure 4.

Abbreviations, SG, subpial granular zone; MZ, marginal zone; CPo, outer cortical plate; CPi, inner cortical plate; SZ, subplate zone; IZ, intermediate zone; SZo, outer subventricular zone; SZi, inner subventricular zone; VZ, ventricular zone.